CHAPTER

Anticorrosion by photocatalytic cathodic protection

26

Daoai Wang and Zia Rahman

State Key Laboratory of Solid Lubrication, Lanzhou Institute of Chemical Physics, Chinese Academy of Sciences, Lanzhou, P.R. China

26.1 Introduction

Metals are extensively used in the construction of buildings, pipelines, aircrafts, ships, offshore equipment, bridges, and so on. However, metals are destroyed by corrosion causing huge economic losses, environmental pollution, and disastrous accidents. Stainless steel, an engineering material, has been widely used because of its hardness, stability, high resistance to temperature, and corrosion. But it is also prone to severe corrosion when exposed to moist environment or water containing chloride ions. In a recent report, the global cost of corrosion was estimated to be US$2.5 trillion which is almost 3.4% of the global gross domestic product [1].

It is therefore need of the day to protect metallic structures from corrosion. In the past decades, many strategies have been developed to inhibit corrosion. Coating and cathodic protection of metals are the main technologies which are commonly employed for anticorrosion. Coating of various inorganic and organic materials on the surface of metals provides physical barrier which prevent salt, water, and oxygen to reach the surface of metals [2–4]. Thus chemical reactions of these chemical substances with the metal are prevented and corrosion of the later is inhibited. Nevertheless, the organic corrosion inhibitors require complex synthesis procedures and most of them also cause serious environmental pollution. In addition, organic coating is not so stable and minor cracks in coating will lead to pitting corrosion. While repeated coating will result in energy and materials cost making the process expensive and inefficient for large size objects.

Cathodic protection is an efficient and one of the most widely used techniques used for anticorrosion of different structures of metals on the ground, underground, and submerged. In this technique either a sacrificial anode (galvanic) or impressed current is employed to transfer electrons and suppress the oxidation reaction of the metals. In case of sacrificial anode method, active metals (Zn, Mg, and Al) are used to transfer electrons and shift the potentials of protected metals (cathode) to more negative than the corrosion (Fig. 26.1A) [5]. The application of sacrificial anode cathodic protection is restricted by the high cost of anodes and environmental pollution caused by anode materials as these are oxidized and released into environment during the corrosion process. In impressed current cathodic protection, an external power source is utilized to provide electrons to the protected metal which shift its potential to a negative and stable region. It is mainly applied

Smart Anticorrosive Materials. DOI: https://doi.org/10.1016/B978-0-323-95158-6.00006-0

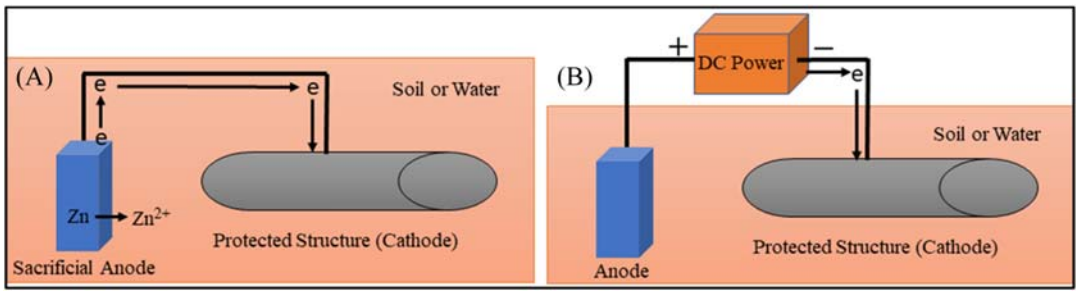

FIGURE 26.1

Schematic diagram of sacrificial anode cathodic protection (A) and impressed current cathodic protection (B).

for metals submerged in water and in soil which provide electrolytic cell conditions (Fig. 26.1B). This technique is also not favorable because of expensive and complicated electronic devices such as batteries, rectifiers, generators, and constant consumption of electric power. It is imperative to seek efficient, cost effective, and green technology to protect metals from corrosion.

Photocatalytic or photocathodic protection (PCP) is a novel and green technology which has been recently used to inhibit corrosion of metals. It is considered to be more advantageous as compared to traditional cathodic protection. This technique utilizes solar energy, which is abundant and green energy, for providing electric current to the metals for cathodic protection. Moreover, during this process, the material (semiconductor) itself is not consumed and is not released into environment making the technique environment friendly.

In PCP technique, a semiconductor photocatalyst is used which is irradiated with light having energy greater or equal to the band gap energy ($h\upsilon \geq E_g$), the electrons in filled valence band (VB) are excited to the empty conduction band (CB) and then injected to the coupled metal through external circuit. The continuous transfer of photogenerated electrons enrich the coupled metal shifting its self-corrosion potential to a negative stable region and results in PCP. During the process, photoinduced holes are also simultaneously generated in VB which have oxidizing properties and are also consumed by reducing species in the medium (Fig. 26.2). The semiconductor itself is not consumed and therefore not released into environment causing no pollution.

The continuous injection of negative electrons to the coupled metal is key factor of this technique. The efficiency of PCP is dependent on semiconductor design, structure and should have some specific characteristics. One of the important requirements is that the CB potential of semiconductor photocatalyst should be sufficiently negative than the self-corrosion potential of coupled metal so that the photoinduced electrons are easily transferred to the latter making it a cathode. In PCP, the photoelectrode semiconductor is usually n-type so it acts as anode and photoanode current is obtained that transfers electrons to the metal which is protected against corrosion. In addition, the photogenerated electron−hole pairs must be effectively separated and their recombination should be inhibited. Holes must be consumed by the hole scavengers present in surrounding medium which are oxidized. In this way, hoes are prevented from recombination with photogenerated electrons. Semiconductor must be chemically stable and not corroded by surrounding medium during the PCP process [6].

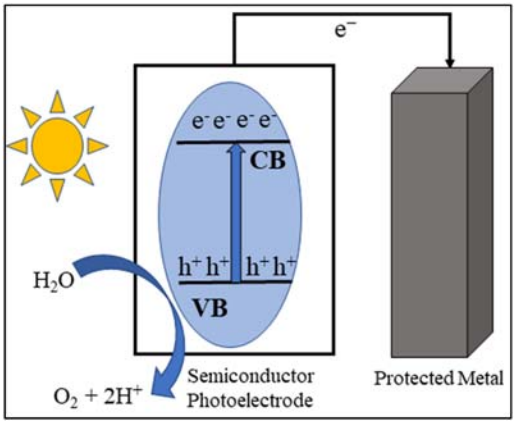

FIGURE 26.2

Schematic diagram of photocathodic protection of metals.

Recently, many researchers have focused on PCP and have developed different semiconductor photoanodes. Since photoanode is the key part of this technique, various types of semiconductor materials have been studied for this technique, such as TiO_2, ZnO, Fe_2O_3, SnO_2, In_2O_3, WO_3, $SrTiO_3$, and g-C_3N_4. Here some recent progress in the development of photoanodes is discussed.

26.2 TiO_2 photoelectrode

Titanium dioxide is n-type of semiconductor material which has been applied in photocatalysis, water splitting, environmental remediation, and solar cells due to its amazing properties such as low cost, low toxicity, high abundance, high stability, photosensitivity, and resistance to corrosion. Yuan and Fujisawa for the first time in 1995 used TiO_2 for the PCP of copper and steel [7,8]. They found that TiO_2 can provide cathodic protection to the coupled metals when illuminated with ultraviolet (UV) light. Since this discovery, TiO_2 has gained special attention and has been widely researched photoelectrode for PCP in the past decades [9–11].

When TiO_2 is irradiated with light having energy equal to or greater than its band gap ($h\upsilon \geq 3.2$ eV), electron–hole ($e^- h^+$) pairs are created. The photogenerated charge carriers are separated. Electrons are excited to the CB and are transmitted to metal through external circuit which shift its open circuit potential (OCP) to a more negative value than its corrosion resulting its protection from corrosion. Photoinduced holes in VB of semiconductor oxidize water and/or organic compounds while semiconductor itself is not decomposed and acts as nonsacrificial photoanode. This is the basic principle involved in photocatalytic anticorrosion of metals.

Although TiO_2 has been extensively studied, its applications in PCP for metals are still limited by its low efficiency when used in pure form. First, its wide band gap ($E_g = 3.2$ eV) makes it to absorb only UV light ($\lambda < 390$ nm) which constitutes <5% of the solar light. Pristine TiO_2 material cannot absorb light in the visible region. Second issue is its fast recombination of photogenerated

charge carriers affecting its photoelectric efficiency. Photogenerated electrons combine with holes, are annihilated, and are not generated in the absence of light. Thus efficient protection of metals from corrosion especially under dark conditions is still a serious challenge. Various strategies have been developed to modify TiO_2 and to enhance its photoconversion efficiency, extend its absorbance to visible region, and inhibit recombination of electron−hole pairs. Some of the strategies include doping with metals and nonmetals, coupling with semiconductors, sensitization with quantum dots, etc. which will be discussed in this section.

26.2.1 TiO_2 surface modification

Various surface treatments have been used to enhance the photoactivity of TiO_2. In one report, TiO_2 nanotube arrays (TiO_2 NTs) were treated with hydrogen at high temperature and pressure to get hydrogenated TiO_2 nanotube arrays (H−TiO_2 NTs) by Wei et al. [12]. It was found that the H−TiO_2 NTs showed red shift to visible spectral region. The prepared NTs were used as photoelectrode for the PCP of 304 stainless steel (304SS). The photoelectrochemical (PEC) results showed that photocurrent density was 4.5 times and 23 times higher than pristine TiO_2, under simulated solar light and visible light, respectively. Moreover, the photoinduced OCP showed a more negative value (−640 mV) and Tafel polarization curves indicated −0.653 V, under simulated solar light, confirming the effective transfer of electrons to 304SS and efficient PCP (Fig. 26.3). The effective protection is due to the fact that hydrogenation produces Ti^{3+} or oxygen vacancy in TiO_2 which results in its narrow band gap and more light absorbance leading to improved cathodic protection.

Similarly, TiO_2 NTs were irradiated with UV light to enhance its PEC property and then applied as photoanode for the PCP of 304SS [13]. The UV-treated TiO_2 NTs photoanode showed 50% more photocurrent density (600 $\mu A/cm^2$) than the pristine TiO_2 under simulated sunlight. OCP results indicated that after 1 h UV illumination NTs showed negative potential of −678 mV versus Saturated calomel electrode (SCE) for coupled steel. Moreover, electrochemical impedance spectroscopy also proved that the corrosion of 304SS was inhibited under solar light irradiation. This enhanced PEC property of UV-treated TiO_2 is mainly due to the creation of hydroxyl groups on its surface which increases the oxidation of water and suppresses the electrons and holes recombination. Surface treatment techniques which modify TiO_2 surface are simple, efficient, and cost effective as these techniques do not require expensive chemicals and complex reactions. These are promising techniques for enhancing the photoelectric activity of TiO_2 and application in anticorrosion.

26.2.2 Doped TiO_2

Doping is one of the promising strategies adopted to shift absorption to visible region and suppress the recombination of photogenerated electrons and holes. This strategy has been widely researched as compared to others for improving PEC performance. The doped elements can change the band gap, create additional energy levels, and oxygen vacancies. The charge carriers are effectively separated and transferred to the surface. The doping elements are both metals and nonmetals which can enhance the PEC activity of TiO_2 as discussed in the following sections.

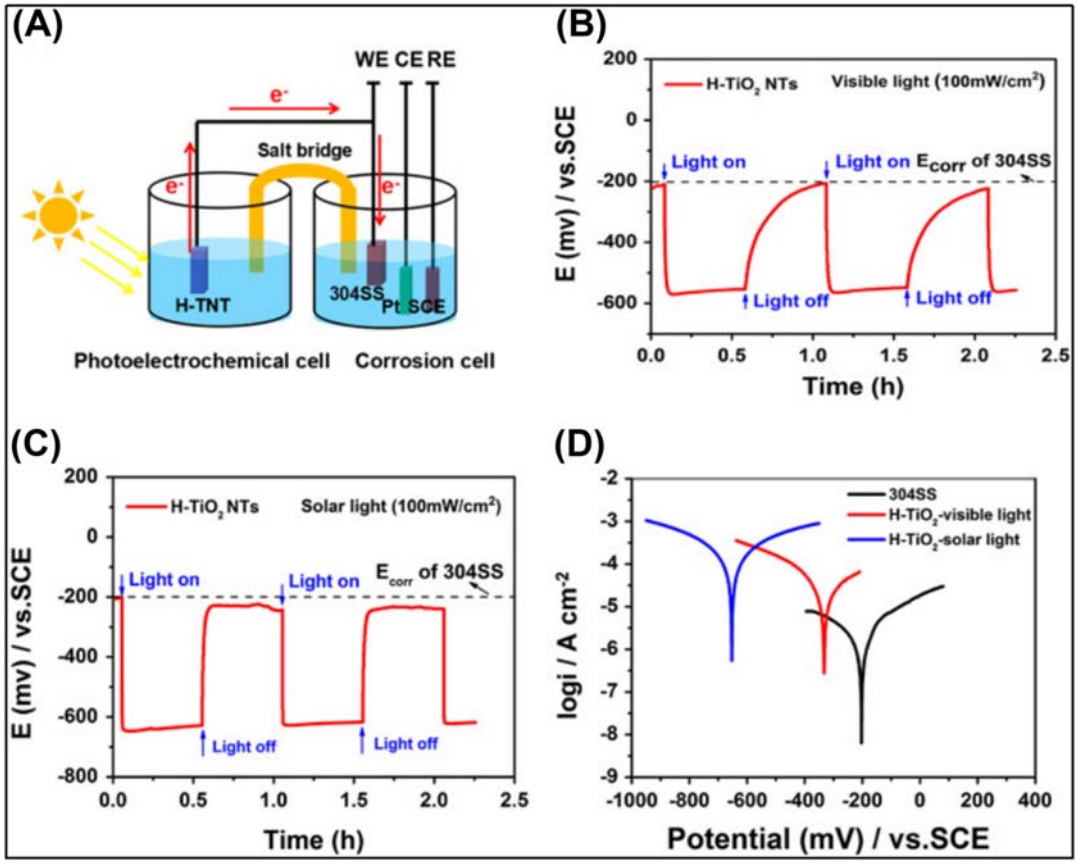

FIGURE 26.3

(A) Schematic of the experimental setup for photogenerated cathodic protection coupled with 304SS. Photoinduced OCP variation of H−TiO_2 NTs under visible light (B) and simulated solar light (C) illumination. (D) Tafel curves of pure 304SS and H−TiO_2 NTs under visible light and solar light [12].

26.2.2.1 Metal doping

A variety of metals such as Fe, Co, Ni, Zn, Cr, Ag, Pt, Mo, Ce, W, and their combinations (codoped) have been reported for doping TiO_2 to enhance its photocatalytic property.

Due to the low cost and ion radius close to Ti^{4+}, Fe is considered a suitable dopant for changing the band gap of TiO_2. Fe-doped TiO_2 films have been fabricated by Liu et al. using iron nitrate as the Fe source though liquid-phase-deposition (LPD) method [14]. The PEC property of Fe-doped TiO_2 films was greatly enhanced as compared to undoped TiO_2. The PCP of 304SS in 0.5 M NaCl was proved by its potential drop (−360 mV) under white light illumination when coupled with Fe-doped photoanode even after the light was turned off ensuring effective cathodic protection. 316SS was also protected from corrosion in 0.5 M NaCl solution under irradiation and dark

conditions using Fe-doped TiO_2 nanotube arrays [15]. The enhanced photocatalytic property of Fe-doped photoelectrodes is attributed to the high absorbance in visible region and low band gap energy. Moreover, oxygen can effectively trap the photoexcited electrons through Fe^{3+} ions in the doped TiO_2 which leads to efficient separation of electron−hole pairs improving PCP.

Similarly, in a recent study, Ag was electrodeposited on Fe-doped TiO_2 nanotube arrays (FeTNTs) to get Ag/FeTNTs. The composite photoanode showed higher absorbance, separation efficiency, and PEC performance of 304SS under light irradiation and dark and shifted its potential to a value of −700 mV [16]. The same group also reported a series of other codoped photoanodes such as the preparation of W and Fe codoped TiO_2 nanotubes (W−Fe-TNTs), Fe−Co−W-TiO_2 nanotube films, Ni−Pt/Fe−TiO_2 nanotube films, and Cr and W codoped (Cr−W-TiO_2) nanotube photoelectrodes [17−20]. The results of OCP, photocurrent density, and Tafel polarization curves indicated effective charge separation and PCP of 403SS, due to the synergistic effect of codoping which also improves the generation and injection of electrons from CB of photoelectrode to the coupled steel. The potential of 403SS was shifted to −530 mV which is far more negative than the corrosion potential of 403SS after attaching with codoped TiO_2.

Ni-doped TiO_2 photoelectrode was fabricated using sol−gel method and applied for the PEC anticorrosion of 304SS [21]. The high photoresponse of the photoanode is because the doping of Ni substitutes Ti^{4+} ions in the lattice and creates oxygen vacancies which result in high photo-to-current conversion efficiency and enhanced PEC property. Similarly, Zn-doped TiO_2 (Zn-TiO_2) films prepared by sol−gel method also indicated better results than pure TiO_2 [22]. Zhang et al. reported the synergy of Mo-doping and heterojunction resulting from rutile/anatase mixed phase can enhance the PEC performance [23]. Mo-doped TiO_2 NTs show more photocurrent density, visible light absorption, and incident photon to current conversion efficiency than pure TiO_2 NTs. This is credited with increased oxygen vacancies and reduced recombination of photogenerated charge carriers by Mo-doping and heterojunction formation in anatase/rutile mixed phase. Due to doping, the band gap is narrowed and oxygen vacancies are formed on the surface of TiO_2 NTs which can trap photoinduced electrons inhibiting their recombination with holes (Fig. 26.4). These factors lead to higher PEC activity of Mo-doped TiO_2 NTs.

Li et al. have also reported Ce-doped TiO_2 and Cr-doped TiO_2 coatings and their anticorrosion property was investigated by coupling with 316L SS in NaCl solution. The effect of metal content on PEC property was investigated which varied with varying percentage of the doped metals.

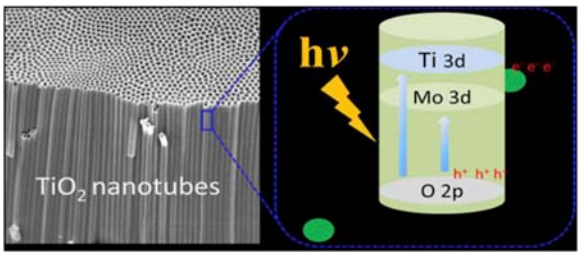

FIGURE 26.4

Schematic illustration for the charge separation of the Mo-doped TiO_2 nanotubes [23].

Results proved that 1.2% Ce-TiO_2 and 1% Cr-TiO_2 coatings showed the best PCP as compared to others. Both Ce^{4+} and Cr^{3+} can trap electrons in the CB under illumination and result in suppressing the recombination of photogenerated electrons and holes. Electrons are thus effectively transferred to the metal shifting its potential to more negative than its corrosion [24,25].

26.2.2.2 Nonmetal doping

Nonmetal doping is also a common strategy which introduces energy levels above VB that results in shortening of band gap. The common nonmetals include N, F, B, S, and their combinations (codoped). Li et al. prepared nanoflower like N-doped TiO_2 (N-TiO_2) films and nanotube arrays using hexamethylenetetramine as a source of nitrogen through hydrothermal method and self-organized electrochemical anodization, respectively [26,27].

The nanoflower like morphology of N-TiO_2 varies with duration of reaction as shown in Fig. 26.5. N-TiO_2 showed significance response to visible light (600−700 nm) and enhanced photocurrent in UV and visible light. This is due to change in band gap and high surface area leading to more photogenerated charge carriers. The strong absorption edge at 650 nm of N-doped TiO_2 corresponds to band gap energy of 1.91 eV, which is much smaller than that of pure TiO_2 (3.2 eV). The electrode potential of 316L SS shifted to negative when coupled with N-TiO_2 electrode under irradiation in 0.5 M NaCl solution and this negative potential was maintained for long time under dark conditions proving its efficient PCP as compared to TiO_2.

Similarly, in a recent report, N-doped TiO_2 particles were prepared using urea as a source of nitrogen. The prepared doped TiO_2 particles not only showed absorption in the visible region but also showed effective potential drop of 3044SS under illumination. This was due to the introduction of new intermediate energy level with band gap energy of 2.1 eV as a result of N-doping which also facilitates excitation of electrons to the CB and separation of electron−hole pairs [28]. Light absorption is enhanced by the formation of intermediate energy level above the O-2p VB and therefore more injection of electrons to metal under light illumination (Fig. 26.6).

Boron-doped TiO_2 nanotubes have been prepared using boric acid a source of boron via in situ anodization [29]. The OCP and Tafel polarization results indicated a potential drop of 403SS when coupled with boron-doped TiO_2 under illumination. The potential drop changed with concentration of boric acid and very high potential drop of −650 mV for BT15 sample (boric acid concentration of 15 mM) was obtained which also showed the highest photocurrent as compared to other samples. The photogenerated cathodic protection is due to large number of electrons which transfer from B-TiO_2 to the coupled steel. Sulfur has also been used for doping TiO_2 to prepare S-doped TiO_2 film photoanode using thiourea as source of sulfur through sol−gel technique [30]. The doped photoanode was used for the PCP of 304SS under light irradiation and the potential was shifted to negative than the corrosion potential even for some time after the light was turned off which indicate the superior performance of the doped TiO_2 photoanode.

Lei et al. have prepared N−F codoped TiO_2 film photoanode for successful PCP of 304SS through LPD method. The doped TiO_2 films indicated response in the visible region (600−750 nm) and increased photocurrent intensities in UV and visible light. The photoeffects of films are due to the synergy of codoped N and F [31].

Although doping can modify the band gap, the absorption efficiency is low. In addition, defects are introduced in TiO_2 which leads to recombination of the photogenerated charge carriers and loss of PEC activity. In order to solve this issue, some other strategies have been suggested.

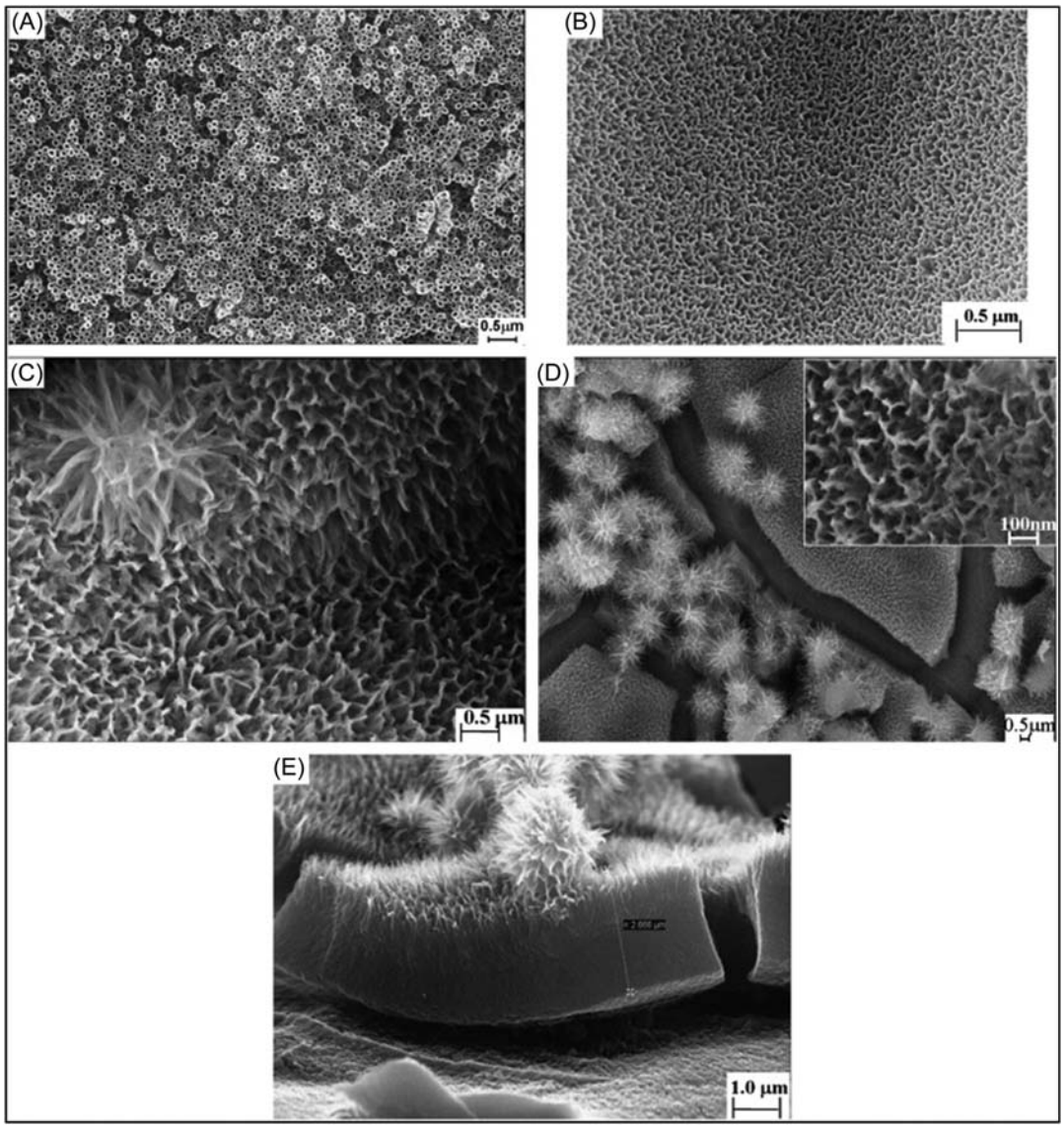

FIGURE 26.5

Typical SEM images of the top (A–D) and cross-sectional view (E) for the TN arrays prepared by electrochemical anodization at 25 V for 5 h (A) and the N-doped flower-like, nanostructured, TiO_2 films with different reaction times. (B) 18 h; (C) 24 h; (D, E) 60 h [26].

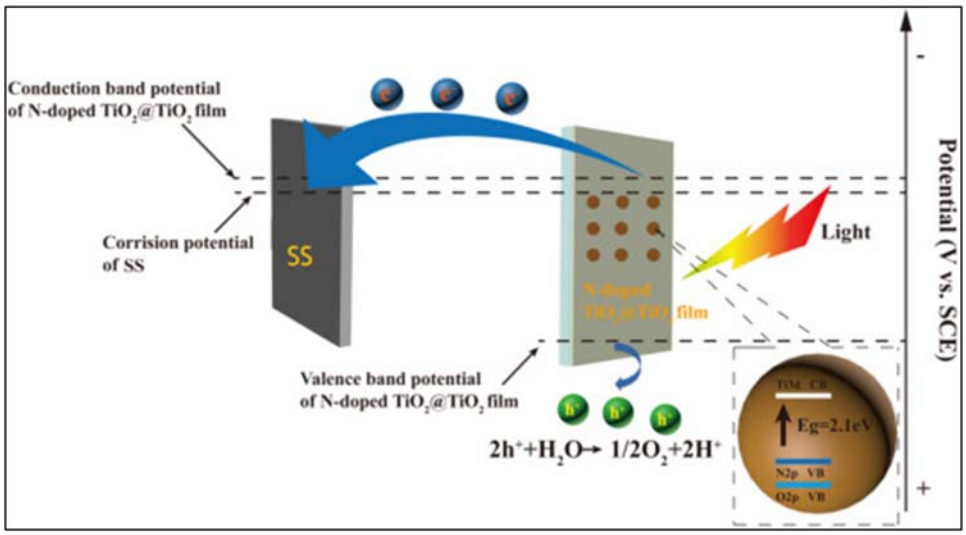

FIGURE 26.6

The photocathodic protection mechanism of N-doped TiO_2@TiO_2 photoanode coupled with stainless steel [28].

26.2.3 Semiconductor coupling

Coupling TiO_2 with other semiconductors is also an effective strategy to improve the separation of electron−hole pairs and hence the PEC property of TiO_2. Many semiconductors have been investigated for coupling with TiO_2. Some of these are discussed here in the following sections.

26.2.3.1 Metal oxide semiconductors

Metal oxide semiconductors have appropriate band gaps which enable TiO_2 to enhance absorbance and its photocatalytic activity. Zinc oxide (ZnO) has been coupled with TiO_2 because of its band gap (3.37 eV) and almost the same position of the VB and CB. As compared with TiO_2, the migration of electrons and holes in ZnO is easier between ZnO and TiO_2. In addition, the mobility of electrons is higher in ZnO than TiO_2 which can improve the separation of photoinduced electron−hole pairs and therefore it is considered to be appropriate for coupling to enhance PCP property of TiO_2. Using sol−gel method, TiO_2/ZnO composite films have been prepared which showed red shift in absorbance, high current density, and efficient PCP property. The potential of 304SS when coupled with composite photoanode dropped to −820 mV under illumination in 3.0% NaCl solution and proved efficient anticorrosion protection [32]. In another report, photoanode of ZnO/TiO_2 was applied for the cathodic protection of 316SS and Q235 carbon steel (CS) in NaCl solution. The OCP of both 316SS and Q235 CS lowered as much as −991 and −1066 mV, respectively [33]. Multilayered ZnO/TiO_2 also exhibited excellent corrosion protection of 304SS in 3% NaCl solution with a protection efficiency of 98% [34]. Recently, ZnO−TiO_2 was coated with polyvinyl chloride (PVC) to give composites of ZnO−TiO_2/PVC. The composite provides anticorrosion self-healing

coating. Anticorrosion performance was studied using CS in 0.5 M HCl + 3.5% NaCl. Results indicated that even after 10 days of exposure the protection capacity was 97.1% [35].

α-Fe_2O_3 with a small band gap (2.1 eV) shows high stability and can be easily prepared. So, it is also suitable for compounding with TiO_2 to improve its photogenerated cathodic protection. α-Fe_2O_3/TiO_2 heterojunction films have been successfully fabricated for improved PCP. The composite photoanode showed lower band gap energy (1.99 eV), higher separation of photogenerated electrons, and superior PCP for 20 steel with 90.3% protection efficiency [36]. Similarly, Fe_2O_3/TiO_2 heterojunction system was applied for enhanced PCP of CS [37]. After modification with Fe_2O_3 the band gap of photoanode became narrow (2.26 eV) improving the harvesting of solar light and photocurrent density increased four times higher than TiO_2. The photoanode exhibited improved PCP behavior for CS under simulated sunlight illumination.

Although NiO has a wide bang gap (3.55 eV), it can build p−n heterojunction with TiO_2. The p−n heterojunction system of NiO/TiO_2 is prepared by electroless plating, which can improve the separation of photogenerated electron−hole pairs [38]. The composite shows higher absorbance in visible region which results in higher photoelectric property. The PCP performance increases shifting the potential of 304SS to more negative (−780 mV) than the corrosion which is attributed to its effective separation of charge carriers. Electrons from n-type TiO_2 migrate to combine with holes from p-type NiO at the heterojunction and results in the creation of build-in field. The photogenerated electrons and holes are effectively separated by the build-in field at p−n heterojunction and result in efficient PEC performance (Fig. 26.7).

Cu_2O is p-type semiconductor with a narrow band gap (2−2.2 eV). It has strong visible light absorbance and has photocatalytic property. Recently, Tian et al. have reported the p−n heterojunction Cu_2O/TiO_2 composite photoelectrode [39]. The PCP performance of the prepared composite photoanode was investigated for 316L SS under visible light. The protection from corrosion of the composite is due to built-in electric field at the interface as a result of p−n heterojunction. The built-in field improves the separation of charge carriers and transfer of photogenerated electrons to 316L SS. In addition, deposition of Cu_2O also increases the number of photoactive sites resulting in efficient PEC performance.

In_2O_3 is a semiconductor with appropriate band structure and visible light responsive behavior. It has negative CB potential with high light absorbance and PEC conversion efficiency. Thus its heterojunction with TiO_2 is favorable to enhance the PCP performance of TiO_2. The PEC cathodic

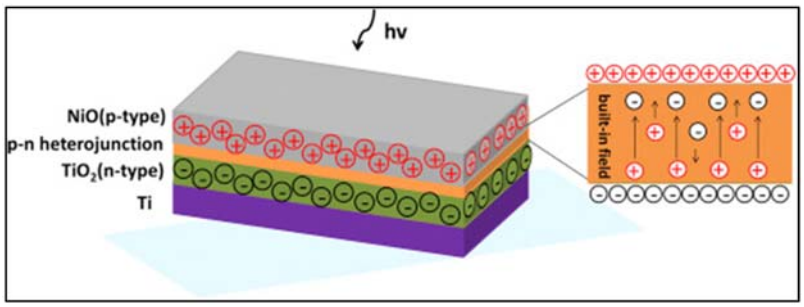

FIGURE 26.7

Illustration of NiO/TiO_2 p−n heterojunction and the electron−hole separation in the built-in field [38].

protection property of In_2O_3/TiO_2 composite is enhanced for 304SS in 3.5% NaCl under white light and visible light which is also attributed to improved separation of electron−hole pairs [40]. The relatively narrow band gap (2.3−2.8 eV), enhanced light absorption, and PEC property make Bi_2O_3 appropriate p-type semiconductor for coupling with TiO_2. The p−n heterojunction at the interface of Bi_2O_3−TiO_2 composite significantly improves the separation of photoinduced electron−hole pairs. The band gap becomes narrow (2.55 eV) and photocurrent density increases. The composite photoanode provides protection to 304SS from corrosion and its potential is decreased to 450 mV [41].

26.2.3.2 Quantum dots semiconductors: sensitization

Since the modification of TiO_2 is the prerequisite for improving the PCP, sensitization is one of the most effective strategies. Sensitization improves light harvesting by extending the light absorption to visible region and separation of photogenerated electron−hole pairs. For sensitization of TiO_2, quantum dots are appropriate sensitizers because of their narrow band gap, unique electrical and optical properties.

CdS is a narrow band gap (2.4 eV) semiconductor and has significant capacity of photoelectron transmission. It is a semiconductor that has been used for modification of TiO_2 to improve its PCP performance. Li et al. reported electrodeposited CdS on TiO_2 nanotube arrays (CdS-TNs) for PCP of 304SS [42]. The composite CdS-TNs film displayed high photoresponse in UV and visible light which is due to efficient charge separation and electron transfer. The potential of 304SS shifted negatively when coupled with CdS-TNs under illumination in NaCl solution and potential remained negative for 24 h after light was cut off which proves its stability and efficiency. Similarly, CdS/TiO_2 composite film, which was prepared by using chemical bath deposition, has been investigated for PCP performance [43]. The relationship between PEC response and corrosion of the composite was also investigated. Composite film displayed higher PEC response compared to pure TiO_2 which is attributed to improved separation of photogenerated electron−hole pairs and their transportation. However, the PEC is affected by the corrosion of composite photoanode.

Selenide (Se) and telluride (Te) are semiconductors that are similar to sulfide. CdSe and CdTe have narrow band gap of 1.74 and 1.45 eV, respectively. These quantum dots show visible light absorbance and have been widely studied as sensitizer of TiO_2. CdTe was coated on TiO_2 nanotubes by Wang et al. using electrochemical deposition method [44]. The absorbance of CdTe/TiO_2 composite was improved, shifted to visible region and the band gap became narrow (2.5 eV). The results of OCP and Tafel polarization curves proved effective PCP of the composite photoanode under light and dark. The prepared photoanode exhibited high photocurrent density of 400 $\mu A/cm^2$. Under visible light illumination, the potential of 304SS when coupled with CdTe/TiO_2 negatively shifted to −850 mV. The stored electrons in the composite can be transferred to coupled steel providing protection under dark condition.

The photoanode of ZnSe/TiO_2 NTs was prepared using cyclic voltammetry electrodeposition technique for the effective PCP of 304SS [45]. The test results of OCP and photopolarization indicated that the composite photoanode under the visible light illumination exhibited significant protection of the attached metal. The shift in potential of 304SS was more negative (−780 mV) when coupled with ZnSe/TiO_2 than coupled to TiO_2, even in the dark which is attributed to the stored photoelectrons. Similarly, $NiSe_2/TiO_2$ nanocomposite photoelectrode exhibited strong photoresponse, high photocurrent density, and effective separation of photogenerated electrons and holes [46]. The nanocomposite photoanode effectively protected 304SS in 3.5% NaCl corrosion solution under visible light. However, the efficiency is affected with $NiSe_2$ amount and excess amount on the surface may cause recombination of electron−hole pairs, and efficiency of electrons transfer to 304SS is lowered. Ni_3S_2 is n-type semiconductor and it also has a narrow band gap (2.5 eV).

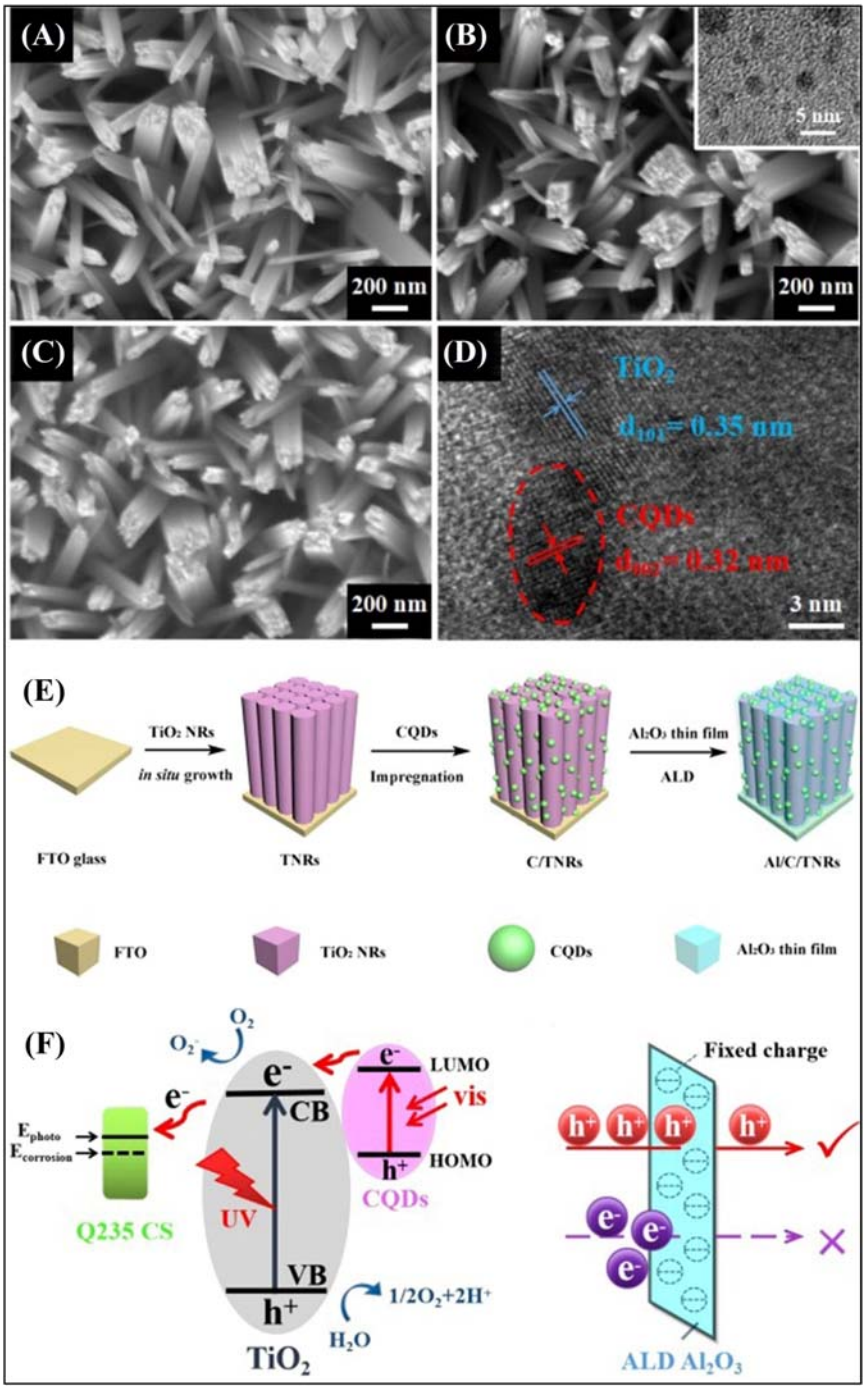

FIGURE 26.8

SEM images of TiO_2 NRs (A), CQDs-loaded TiO_2 NRs (B), CQDs-loaded TiO_2 NRs covered with 5 nm Al_2O_3 layer (C), and high-resolution transmission electron microscopy (HRTEM) image of CQDs-loaded TiO_2 NRs (D). The inset of (B) shows the TEM image of CQDs. (E) Schematic diagram of the procedures of preparing TiO_2 NRs (TNRs), CQDs-loaded TiO_2 NRs (C/TNRs), and Al_2O_3 anchored CQDs-loaded TiO_2 NRs by ALD method (Al/C/TNRs). (F) Schematic representation of the energy band structure and electron transfer processes in CQDs/TiO_2 NRs composite and the role of atomic layer deposited Al_2O_3 layer as filter membrane [57].

Moreover, its both VB and CB are lower than that of TiO_2. A sheet of Ni_3S_2 was coated on TiO_2 nanotubes via hydrothermal method to produce Ni_3S_2/TiO_2 composite photoanode [47]. The photoanode provided effective PCP to 304SS in 3.5% NaCl solution. The composite photoanode is n-type semiconductor generating photoelectrons under light which are transferred to the surface of coupled steel shifting its potential to more negative (−720 mV) under visible light illumination. The potential was still negative after light was turned off.

Because of its narrow band gap (1.3 eV) and visible light, harvest Bi_2S_3 can be coupled with TiO_2 for enhanced PEC property. Bi_2S_3/TiO_2 heterojunction system has improved visible light absorbance, high photocurrent density, and efficient separation of photogenerated electron−hole pairs [48,49]. The photogenerated electrons are easily transferred composite photoanode to the surface of 304SS decreasing its electrode potential to −675 mV and its corrosion is suppressed. Similarly, Bi_2Se_3, which is narrow band gap and n-type semiconductor, has high electrical conductivity and is considered appropriate for coupling with TiO_2. The nanocomposite of Bi_2Se_3/TiO_2 has a high photocurrent density (415 $\mu A/cm^2$) superior PCP performance as compared to pure TiO_2. The potential of 304SS is remarkably decreased to 996 mV when coupled with Bi_2Se_3/TiO_2 nanocomposite photoanode [50]. Sensitization of TiO_2 by Ag_2S has also attracted attention. It is a narrow band gap semiconductor and its CB is higher and VB is lower than that of TiO_2. It can extend the absorption of TiO_2 to visible range, improve the separation of electron−hole pairs, and chare carrier transfer. Ag_2S/TiO_2 composite has shown enhanced visible light absorption and PEC property than pure TiO_2. The composite photoanode exhibited excellent corrosion protection of 304SS under light shifting its potential to more negative (−907 mV) [51,52]. Similarly, as narrow band gap p-type semiconductors, PbS, MnS, and SnS have also been reported for sensitization of TiO_2. The composite photoanodes with p−n heterojunction structure have displayed enhanced light absorption, photocurrent density, separation of photoinduced charge carriers, PEC performance, and excellent PCP for 304SS [53−55].

Recently, graphene quantum dots (GQDs) have also been reported as a sensitizer of TiO_2, due to its continuous absorption of UV−visible light and high conductivity. GQDs sensitized TiO_2 nanotube arrays (GQDs/TNAs) photoelectrode displayed high light harvesting and extended absorption to visible region. It exhibited a high photocurrent density (800 $\mu A/cm^2$) and significant PCP for 304SS under illumination decreasing its potential to 740 mV. The remarkable PCP performance of $GQDs/TiO_2$ can be attributed to its superior separation and transfer of photogenerated carriers [56].

Carbon quantum dots (CQDs) are new type of efficient sensitizer which can produce large number of electron−hole pairs under light irradiation. In addition, its lowest unoccupied molecular orbital energy level is higher than the CB of TiO_2 which facilitates the transfer of electrons to CB of TiO_2. Feng et al. recently reported Al_2O_3 anchored CQDs for sensitization of TiO_2 by fabricating CQDs-loaded TiO_2 nanorods array (Al/C/TNRs) to increase its PEC property (Fig. 26.8) [57]. The absorbance of photoanode was extended to visible region after loading CQDs and photocurrent density reached to a very high (2.28 mA/cm^2) value. The C/TNRs photoanode exhibited excellent PCP of Q235 CS. The potential of Q235 CS decreased to 620 mV in 3.5% NaCl solution under simulated solar light and remained negative for 7 h after illumination as shown in Fig. 26.9.

As mentioned earlier, quantum dots can enhance spectral absorption and transfer of carriers. But the agglomeration and photocorrosion of quantum dots will severely affect PCP of the composite photoanode when used as single sensitizer. Therefore cosensitization strategy can enhance the stability and PCP performance of the composite photoanode. CQDs and Ag nanoparticles (NPs)

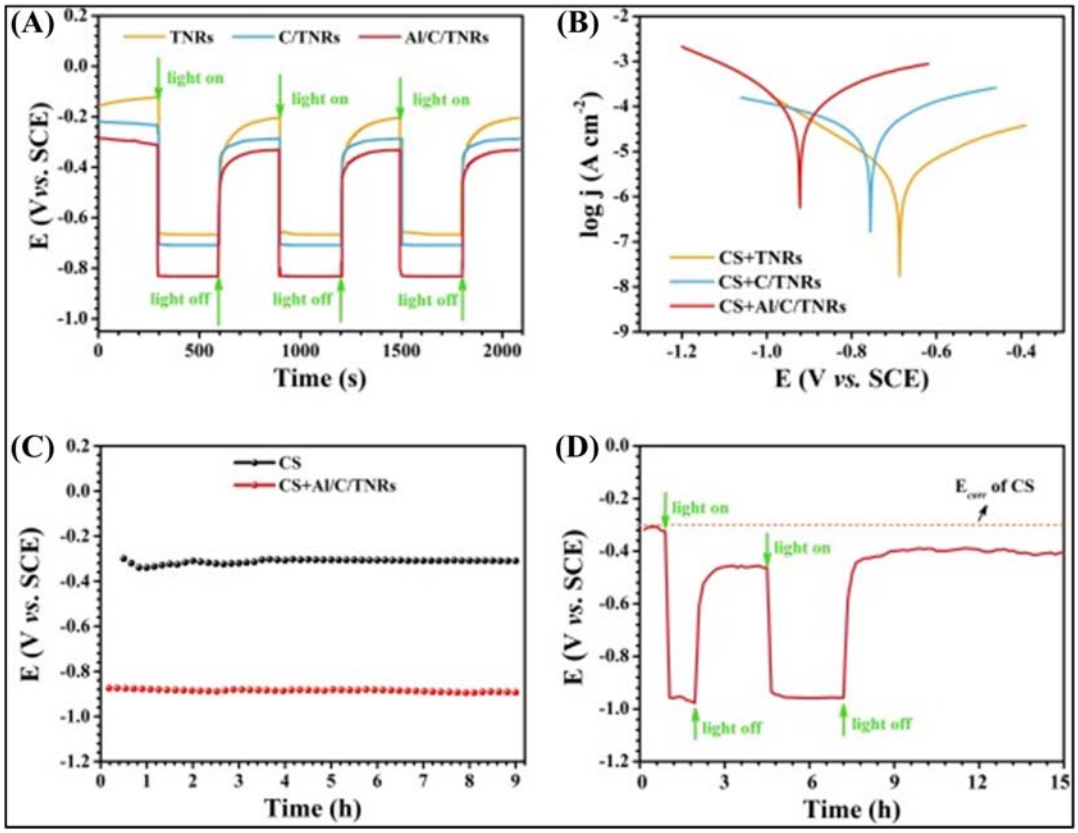

FIGURE 26.9

(A) Photoinduced OCP variation of TiO_2 NRs (TNRs), CQDs-loaded TiO_2 NRs (C/TNRs), and Al_2O_3 anchored C/TNRs (Al/C/TNRs) photoelectrodes, (B) Tafel curves of Q235 carbon steel (CS) electrode connected with TNRs, C/TNRs, and Al/C/TNRs, (C) OCP of Q235 CS electrode before and after connecting with Al/C/TNRs, and (D) OCP changes of Q235 CS electrode coupled with Al/C/TNRs in 3.5 wt.% NaCl solution under simulated sunlight illumination (AM 1.5 G, 100 mW/cm^2) [57].

cosensitized TiO_2 nanotube array (NTA) composite photoanode has been reported. The prepared CQDs/Ag/TiO_2 composite exhibited enhanced light absorption which extended to visible region and PEC performance due to the surface plasmon resonance (SPR) of Ag NPs and upconversion property of CQDs. The photocurrent density of the composite was also four times higher than TiO_2. PCP of the cosensitized photoanode was tested for 403SS in NaCl solution under irradiation and indicated improved PCP effect which is attributed to the synergistic effect of both Ag NPs and CQDs. Li et al. reported the construction of CdSe/reduced graphene oxide (RGO)/TiO_2 and CdTe/graphene/TiO_2 composite photoanodes [58,59]. Both composite photoelectrodes showed higher

light absorption in visible region, higher photocurrent density (560 and 900 $\mu A/cm^2$), and more effective PEC property than pure TiO_2. The PCP performance of photoanodes was investigated using 304SS in NaCl solution by coupling with CdSe/RGO/TiO_2 and CdTe/graphene/TiO_2 which shifted the potential of 304SS, respectively, to −910 and −750 mV. This effective PCP is attributed to the presence of graphene with its fast collection and transfer of electrons.

Both PbS and CdS quantum dots have been deposited on graphene-doped TiO_2 nanosheets (NSs) to prepare cosensitized GT/PbS/CdS composite photoanode. The GT is graphene/TiO_2 nanosheets composites [60]. The composite exhibited high photocurrent density, light harvest, improved separation of photogenerated chare carriers. The composite was investigated for PCP of 304SS under light and dark conditions. The OCP results showed a drop in potential to as low as −839.3 and −632.3 mV under illumination and dark, respectively. The effective PCP performance of the composite is due to the synergistic effect of all components. The PbS and CdS expanded light absorption to visible region. The p−n heterojunction promotes the separation of charge carriers and Schottky barrier at the semiconductor/metal interface promotes transfer of electrons to the coupled metal effectively suppressing its corrosion.

In order to improve the efficiency of photoelectron conversion and transmission, a quaternary photoelectrode of TiO_2 NSs/CdSe/polyaniline/graphene was recently reported [61]. Since graphene has a band gap of zero, high electrical conductivity, and large surface area, it can be used as medium for transmission of electrons from semiconductor to metal. Similarly, the coupling of polyaniline (PANI) can also improve PEC performance by improved transfer of holes and inhibition of charge carriers' recombination. The photocurrent density of the composite photoanode was 6.8 times higher than pristine TiO_2. The OCP and Tafel results proved efficient PCP performance for 304SS shifting its potential to −844 mV. PCP lasted for 4 h after the light was cut off indicating its stability and energy storage ability. The PEC conversion efficiency of the prepared photoanode of $AgInS_2/In_2S_3$ cosensitized TiO_2 nanotube array (NTA) is reported to be higher than that of single QD sensitized TiO_2 [62]. In TiO_2 NTA/$AgInS_2/In_2S_3$, $AgInS_2$ is photosensitizer while In_2S_3 is buffer layer and heterostructure results in rapid separation and transmission of electrons. The photoinduced electrons are transferred to 316L SS when coupled with composite photoanode and provide superior cathodic protection (Fig. 26.10).

Two types of cosensitized photoanodes with noble metals, ZnS/Au/TiO_2 and ZnS−CdS−Ag@TiO_2, have been prepared by Zhu et al. for effective PCP of 403SS [63,64]. Because of very high photocurrent density (19.97 mA/cm^2) and visible light absorption, PEC performance of photoanodes enhanced remarkably. ZnS shell can prevent the leakage of electrons from the surface of metal NPs due to their higher CB. 403SS showed a tremendous decrease in potential (−1174 mV) after coupling with ZnS−CdS−Ag@TiO_2 under light irradiation and also in the dark condition. Zhang et al. have reported the construction of two types of cosensitized photoanodes, CdTe/ZnS/TiO_2 and ZnS/CdSe/CdS/TiO_2 [65,66]. In both of these sensitized photoanodes, ZnS was coated an outer shell to improve the stability of QDs. The photoanodes not only showed stability but also higher photocurrent density, photoabsorption in the visible region, and excellent PCP effect for 403SS in NaCl solution. The OCP results indicated that the potential of 403SS decreased to 400 mV and 1100 under light illumination when coupled with CdTe/ZnS/TiO_2 and ZnS/CdSe/CdS/TiO_2, respectively. The potential was still lower than the corrosion for long time even after the light was cut off proving efficient PCP performance.

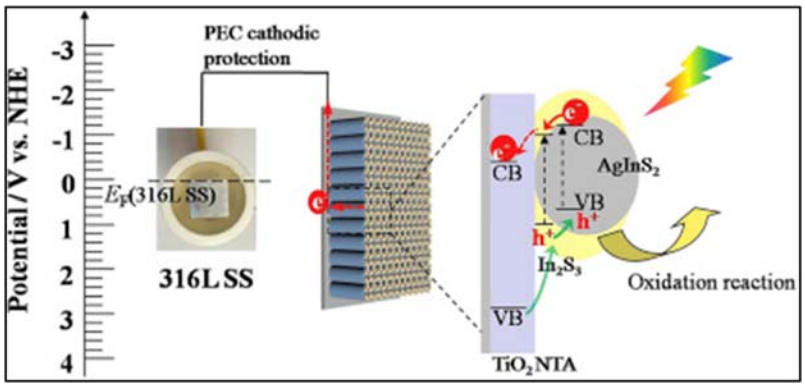

FIGURE 26.10

Proposed mechanisms for the enhanced PEC conversion property as well as the enhanced PEC cathodic protection performance of TiO_2 NTA/$AgInS_2$(3)/In_2S_3(5) under visible light illumination. (The Fermi level of 316L SS is approximately −0.07 V vs NHE.) [62].

A platelike ZnS/Bi_2S_3/TiO_2/WO_3 composite with enhanced PEC performance and energy storage ability has been reported [67]. In this composite photoanode WO_3 serves as energy storage material, TiO_2 buffer layer, and ZnS−Bi_2S_3 a photosensitizer. The structure of the composite results in smooth and gradual transmission of photogenerated electrons from CB of Bi_2S_3 to CB of WO_3 via TiO_2 and then to the coupled metal. The composite photoanode exhibited PCP for 403SS under white light illumination negatively shifting its potential to 540 mV than its corrosion potential. Cathodic protection lasted for 18 h in the dark which is attributed to charge storage ability of the composite photoanode.

26.2.3.3 Energy storage semiconductors

PCP is one the most effective techniques to protect metals from corrosion using photosensitive semiconductors. However, the process takes place only in the presence of light while under dark conditions the process stops and the metal is no more protected because no electrons are generated in the absence of light. The process must be maintained also under dark so that continuous effective protection is provided. To maintain the process sustainable under dark continuous supply of electrons to the metal is essential. This issue can be resolved by coupling photoelectrode with suitable materials having energy storage ability. The composite photoanode from coupling will result in a system of both PEC cathodic protection and energy storage. In the presence of light, the photogenerated electrons are transferred to metal from semiconductor while the extra electrons are stored by the energy storage material acting as electron pool, which are subsequently released and transferred to the metal under dark. Thus the coupled system can provide continuous cathodic protection to the metal. Moreover, coupling TiO_2 with energy storage materials can also reduce the recombination of charge carriers which further enhances PEC property. In order to work effectively, the energy storage materials should have redox activity, with a more positive redox potential than the semiconductor, negative than the CB of the metal and stability. Energy storage materials

are oxides of metals showing multivalency such as WO_3, SnO_2, CeO_2, MoO_3, and V_2O_5 which have been widely studied in the field of PCP. Moreover, the CB of these materials is found to be more positive than that of TiO_2 and negative than the corrosion potential of steel making these materials appropriate for coupling with TiO_2 for enhanced PEC property.

Among these storage materials, Tungsten trioxide (WO_3) is considered most promising due to its narrow band gap (2.6 eV), response in visible light, and its band structure which matches that of TiO_2 facilitating the transfer process. Under light illumination, the photogenerated electrons are excited to the CB of TiO_2 and are injected to the metal cathodically polarizes it. The excess electrons are transferred to the CB of WO_3 because of its lower CB potential than that of TiO_2 which are stored due to the reduction reaction as follows:

$$WO_3 + xe^- + xH^+ \rightarrow H_xWO_3 \tag{26.1}$$

When the light is cut off, the above reaction reverses and electrons stored in WO_3 can be released and transferred to metal providing continuous corrosion protection.

Zhou et al., using sol−gel technique, prepared a photoanode of TiO_2/WO_3 bilayer coatings on 304SS for anticorrosion [68]. The PCP efficiency of the prepared material was evaluated for 304SS in NaCl solution which varied with the coating layers of TiO_2 and WO_3. The results indicated that best performance was obtained for TiO_2/WO_3 with four TiO_2 and three WO_3 layers which reduced the potential of 304SS and maintained its protection for 6 h after UV light illumination for 1 h. Similarly, in another report, the composite film of WO_3/TiO_2, prepared by electrodeposition of WO_3 NPs on TiO_2 nanotubes, shows higher absorption in the visible region and PEC activity than pure TiO_2 [69]. The protection of type 403SS lasted for as long as 19 h after for 2 h light illumination which is credited to the electron storage ability of the composite. Composite hierarchical nanoflake surface of $WO_3@TiO_2$ on FeW alloys covering 316SS, with double protection of PCP and superhydrophobicity, has been prepared by Yu et al. [70]. Excellent anticorrosion performance for 316SS indicated by the material is attributed to its synergistic effect of superhydrophobicity that prevent corrosive chemicals from contacting with metal and PCP of composite heterojunction that continuously provides electrons to the metal in self-discharging. Sun et al. fabricated three-dimensional (3D) WO_3 NPs on one-dimensional (1D) TiO_2 nanotube arrays (TiO_2 NTs/WO_3) through hydrothermal method [71]. The composite electrode exhibited photoresponse in the visible light, higher photocurrent density of 2.5 mA/cm^2, and PCP performance. The OCP results showed potential drop of 304SS to 260 mV under light and remained negative for long time under dark (Fig. 26.11). The efficient PCP is attributed to the effective separation of photogenerated charge carriers owing to visible light responsive WO_3 and combination of 1D TiO_2 NTs and 3D hierarchical WO_3. Under visible light illumination, electrons in WO_3 are excited to its CB, leaving holes in VB which oxidizes water while VB potentials become high. Photoinduced electrons are then transferred to the CB of TiO_2 and VB potential of WO_3 resumes. This results in efficient separation of electron−hole pairs (Fig. 26.11D).

The unique properties of graphene such as high conductivity, stability, and surface area make to further enhance the PCP performance of WO_3/TiO_2 composite. The resultant RGO/WO_3/TiO_2 composite indicated more absorption in UV and visible region. The efficiency as a photoanode was proved from the OCP and Tafel curves which showed a decrease in potential of coupled 304SS under light [72]. The shift in potential was more for RGO/WO_3/TiO_2 (−760 mV) than both WO_3/TiO_2 and TiO_2, under visible light illumination. Under dark condition, the potential of coupled steel

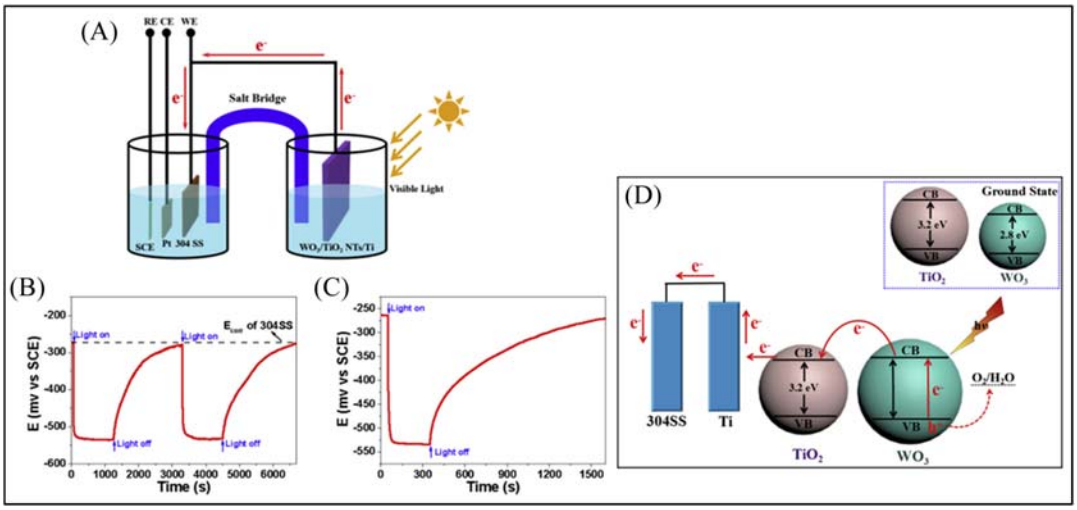

FIGURE 26.11

(A) Schematic of the experimental setup for photogenerated cathodic protection coupled with 304SS. (B) Photoinduced OCP variation of 304SS electrode connected with TiO_2/WO_3 composite under intermittent illumination with visible light. (C) Variations in the potentials of 304SS electrode coupled with TiO_2/WO_3 photoelectrode under initially 360-s illumination by visible light and subsequently >1200 s in the dark. (D) Mechanism of the electron transfer process in the TiO_2/WO_3 composite photoanode coupled with protected 304SS under visible light [71].

still remained −510 and −290 mV with $RGO/WO_3/TiO_2$ and WO_3/TiO_2, respectively. The higher PCP is due to the conductivity of graphene and heterojunction resulting from WO_3/TiO_3 composite which leads to effective charge separation.

Recently, an outer layer of $BiVO_4$ was deposited on WO_3/TiO_2 to enhance its visible light absorption due to its narrow bang gap (2.5 eV) [73]. In the prepared $WO_3-TiO_2-BiVO_4$ composite photoanode, outer layer of $BiVO_4$ promotes visible light absorbance, bottom layer of WO_3 acts as energy storage system, and TiO_2 improves the charging efficiency of WO_3. Under visible light illumination, electrons generated in $BiVO_4$ are transferred to WO_3 and are stored. A part of the electrons is transported to 304SS and cathodically polarizes it by 300 mV. Under dark, the rest of photoelectrons are released to 304SS moving its cathodic polarization to 130 mV and protection is maintained even in the dark.

Tin dioxide (SnO_2) is n-type semiconductor with PEC properties similar to that of TiO_2. It has more electron mobility than TiO_2, its CB is lower than that of TiO_2 and can be used as an electron pool. Therefore coupling SnO_2 with TiO_2 can effectively enhance its PCP in dark owing to its electron storage ability. Under illumination, the excess photogenerated electrons can be transferred to SnO_2 from TiO_2, which are subsequently released when there is no light. The effect of SnO_2/TiO_2 photoanode on the PCP was investigated by Subasri et al. [74,75]. It was found that the composite photoanode with Sn:Ti having molar ratio of 1:1 exhibits highest photocurrent density and is the best one for PCP of copper. The SnO_2-TiO_2 photoanode after irradiation with UV of 4 h can

provide cathodic protection to metal for many hours even after the light was tuned off which is attributed to energy storage ability. The charging process is as under

$$SnO_2 + xe^- + xM^+ \rightarrow M_xSnO_2 (M = H,\ Li,\ \text{or Na and } x = 1 \text{ or } 2) \tag{26.2}$$

In dark condition, the above reaction is reversed and the stored electrons are released and transfer to 304SS providing protection again.

Zhou et al. also investigated the effect of two types of coatings (TiO_2/SnO_2 and TiO_2-SnO_2) prepared on 304SS through the sol–gel method for their energy storage and anticorrosion property [76]. TiO_2/SnO_2 composite provided better corrosion protection to 304SS for prolonged to 7 h under after 1 h irradiation with UV light than that of TiO_2-SnO_2 which lasted for 0.5 h. The results indicated that the better corrosion protection performance of TiO_2/SnO_2 is due to its slow self-discharging time which leads to sustainability.

Zhang et al. prepared nanoflower like composite photoelectrode of SnO_2-TiO_2 by depositing SnO_2 NPs on TiO_2 nanotube arrays (NTs) as shown in Fig. 26.12 [77]. SnO_2-TiO_2-NTs composite electrode, due to it efficient chare separation ability, exhibited four times higher photocurrent density than pure TiO_2. The electrode can successfully protect 304SS in NaCl solution when coupled with electrode. SnO_2-TiO_2-NTs composite electrode under UV irradiation shifted the potential of 304SS to a value of -730 mV higher than TiO_2-NTs which is -670 mV. Although the electrode provides efficient corrosion protection under light, the efficiency in dark condition is not high due to the rapid recombination of photogenerated electron–hole pairs and arrangement of structure.

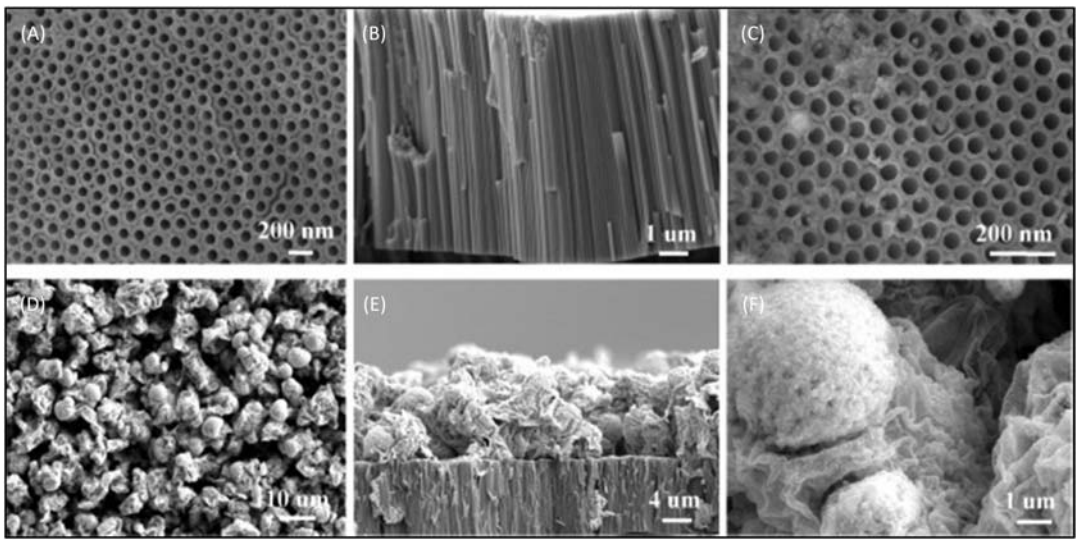

FIGURE 26.12

SEM images of the top view (A) and cross-sectional view (B) of TiO_2-NTs before and after (C) deposition of SnO_2 nanoseeds, and the cross-section view (E) and top view (D), (F) of nanoflower like SnO_2-TiO_2-NTs nanocomposite [77].

The synergistic effects of graphene and SnO_2 have been combined to enhance the PCP performance of TiO_2 [78]. The photocurrent density of RGO/SnO_2/TiO_2 composite (310 $\mu A/cm^2$) was more than pure and varied with graphene content. The PCP effect composite photoanode with heterojunction was studied for 304SS and indicated efficient protection against corrosion. The electrode potential of 304SS dropped by 590 mV when illuminated with white light and remained negative than its corrosion potential for long time in the absence of light. The RGO acts a mediator and transfers the electrons from TiO_2 to SnO_2 enhancing the separation of electron−hole pairs. The electrons can be rapidly transported to metal owing to high conductivity of the RGO.

In order to enhance the visible light absorption and PEC performance, Ag and SnO_2 cosensitized TiO_2 photoanode has been prepared [79,80]. The cosensitized photoanode (Ag/SnO_2/TiO_2) is capable more light absorption with red shift in the visible region, higher photocurrent density, and PEC performance than pristine TiO_2. It also showed PCP performance due to the synergistic effect of SPR of Ag NPs and energy storage ability of SnO_2. In addition, the composite also improves separation and transmission. Under light irradiation, the electrons are transferred from TiO_2 to WO_3, from WO_3 to Ag, and in the last to the coupled metal (Fig. 26.13). The enhanced PCP performance of the composite photoanode was confirmed from the OCP results of coupled steel under white light illumination. A negative shift in potential of −390, −440, and −540 mV was obtained when attached to TiO_2, SnO_2/TiO_2, and Ag/TiO_2, respectively. A negative shift of very high value (−990 mV) was obtained in case of Ag/SnO_2/TiO_2. In the dark condition, cathodic protection can be maintained for more than 19.5 h which is credited to energy storge capacity of composite photoanode.

Cerium dioxide (CeO_2) is n-type semiconductor with bang gap of 2.9 eV. It is more photostable and can be excited by visible light and has widespread applications in photocatalysis. Multiple valences exhibited by CeO_2 indicate its energy storage capability. The redox reaction Ce^{4+}/Ce^{3+} is responsible for electron storage ability. The CeO_2-based photoelectrode will be effective for PCP due to energy storage ability. Bilayer coatings of outer TiO_2 layer and inner CeO_2 layer on copper to construct Cu/CeO_2/TiO_2 and investigate the PEC property of this photoanode have been reported [81]. The outer layer of TiO_2 generates electrons under light illumination and transport to substrate through CeO_2 layer, greatly facilitating the charge transfer owing to its high conductivity. The photoanode exhibits strong energy storage ability due to the in situ reduction of Ce^{4+}. The self-discharge results in sustainable PCP performance.

Molybdenum trioxide (MoO_3) is also n-type semiconductor with a narrow band gap (2.85 eV) and has greatly enhanced visible light PEC and photocatalytic performance of TiO_2. As an energy storage material MoO_3 has been deposited to modify TiO_2 nanotube [82]. The absorption edge of MoO_3/TiO_2 composite red shifted and photoelectric conversion efficiency also enhanced as compared to TiO_2. When attached with MoO_3/TiO_2 composite, the potential of 403SS decreased to 540 mV and under dark condition the potential remained negative for 15 h providing continuous protection in corrosive NaCl solution.

Vanadium pentoxide (V_2O_5) semiconductor can also store electrons and cations in its lattice structure and is widely applied in energy storage devices. TiO_2/V_2O_5 composite can provide enhanced PCP to 304SS under illumination in 3% NaCl solution than TiO_2−V_2O_5 and pure TiO_2

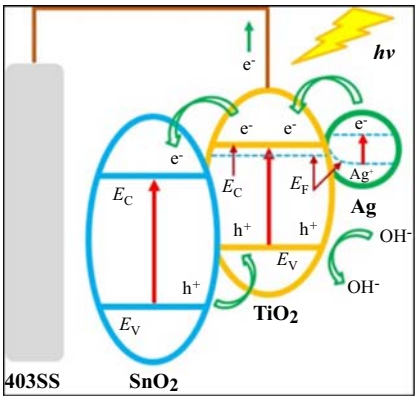

FIGURE 26.13

Illustration of charge separation and transfer mechanism for the $Ag/SnO_2/TiO_2$ composite film under illumination [80].

[83]. The protection is maintained even for 6 h in the dark due to its electron storage property and slow self-discharging time. The charging of V_2O_5 takes place as follows:

$$V_2O_5 + xe^- + xM^+ \rightarrow M_xV_x^{4+}V_{2-x}^{5+}O_5\ (M = H^+, Na^+) \tag{26.3}$$

26.2.4 Carbon-modified TiO_2

As discussed earlier, different strategies have been adopted to increase the PCP efficiency of TiO_2 by modifying the band gap, enhancing the visible light absorption, and photoconversion efficiency. However, the charge transfer efficiency is a key factor and should also be enhanced for effective PCP. The high efficiency of charge transfer will lead to injection of more electrons to the metal decreasing its potential to more negative and more corrosion protection. Carbon and graphene have excellent electrical, mechanical, and thermal properties. These materials show remarkable charge mobility and can enhance the PCP of TiO_2.

Modification with carbon materials such as carbon nanotubes (CNTs) not only improves the charge transfer but also charges separation. Liu et al. reported CNT/TiO_2 composite photoanode for cathodic protection of 304SS under UV irradiation in chloride solution of NaCl [84]. Due to the high conductivity and 1D structure, CNTs provide directional transfer of electrons to the metal. The photocurrent density of composite is three times more than TiO_2. From electrochemical results, it is found that composite photoanode exhibited better anticorrosion protection than TiO_2. From OCP results, it is shown that CNT/TiO_2 decreases the potential of 304SS more (−610 mV) than pure TiO_2 (−365 mV). This is attributed to its high charge transfer to metal substrate on one hand and suppression of electron−hole pairs recombination on the other hand. Moreover, under the dark condition, the potential was lower than the corrosion potential of 304SS.

Among the carbon materials, graphene has attracted special attention due to its amazing properties such as high surface area, stability, and conductivity. Its conductivity is very high with zero band gap and therefore provides it with high charge transfer ability while its two-dimensional structure makes it efficient electron acceptor. It is therefore considered an appropriate candidate to improve the PCP of TiO_2. The composite photoanode of graphene/TiO_2 has shown very high (14 times higher than TiO_2) photocurrent density due to its conductivity and good interfacial contact with TiO_2. It was investigated for PCP of 304SS in 3.0% NaCl solution under illumination and dark condition [85]. The PCP effect of electrode was greatly improved after modification with graphene. In case of composite photoanode, the decrease in potential was higher (−600 mV) than pure TiO_2 (−350 mV) under UV illumination. Zhang et al. found that the enhanced PCP effect of the composite is not only due to improved separation and transport of charge carriers but also diphasic crystalline structure of TiO_2 [86]. Electrons are trapped in space-charge separation region which is created as a result electrons transmission from brookite to anatase and leads to improved separation of electron−hole pairs. From the results of Mott-Schottky, it is evident that graphene causes decrease in Schottky barrier between the interface of TiO_2 and metal, which results in injecting more electrons to its surface. The PCP of graphene/TiO_2 can be enhanced further by incorporating Ag NPs to fabricate Ag/graphene/TiO_2 cosensitized composite photoanode [87]. Graphene not only enhances mobility of charges but also provides support to Ag NPs and prevents their aggregation. Ag NPs further enhanced light absorption and the edge absorption was red shifted to visible region. The photocurrent density of Ag/graphene/TiO_2 enhanced as compared to TiO_2. Composite photoresponsive electrode provided effective PCP to 304SS in NaCl solution under visible light decreasing its electrode potential more (640 mV vs SCE) as compared to graphene/TiO_2 (400 mV vs SCE), Ag/TiO_2 (330 mV vs SCE), and TiO_2 (130 mV vs SCE). The potential of 304SS was still far below than its corrosion for long time (10 h) even after the light was cut off. These results demonstrate the enhanced PCP of Ag/graphene/TiO_2 which is credited to the synergistic effect of enhanced light absorption and charge separation.

26.2.5 Polymer-modified TiO_2

Some polymers can also be used for TiO_2 modification which can improve its PCP performance. These polymers are usually p-type semiconductors with high conductivity and stability. In addition, their visible light absorption and energy storage properties can greatly enhance PEC activity of TiO_2. Under visible light, the photogenerated electrons in p-type polymers can be injected to the CB of n-type TiO_2 separating the electron−hole pairs. The p−n junction between polymer and TiO_2 promotes the separation and transportation of charges. The photogenerated electrons are subsequently injected to the coupled metal resulting negative shift in its potential and provides effective cathodic protection.

Polypyrrole (PPy) is a p-type semiconductor with high stability, high mobility of charges, and conductivity. Its narrow band gap (2.2 eV) leads to absorbance in the visible region and injection of photogenerated electrons into CB of TiO_2. The electron−hole pairs are separated and photoconversion efficiency is enhanced. Cui et al. by electrodeposition of PPy nanowire on TiO_2 nanotube prepared the composite photoanode PPy NW/TiO_2 NT having coaxial heterojunction structure [88]. The composite electrode shows light response in the visible region, high photocurrent density (60.5 $\mu A/cm^2$) and shift in potential. This photoanode can provide efficient corrosion protection to

304SS in NaCl solution under visible light. The OCP of 304SS shows more negative (−0.14 V vs SCE) when couple with composite electrode than that of pure 304SS (0.20 V vs SCE). The negative shift was maintained for long time of 10 h (Fig. 26.14). This effective corrosion protection is attributed to the dual function of the photoanode with PCP and corrosion resistance due to passivation by PPy.

Similarly, in another investigation, it was found that PPy can act as phtotosensitizer and pool for accumulation of photogenerated electrons [89]. The photoanode of PPy/TiO_2 demonstrated enhanced PEC performance and effective PCP of Q235 CS under light and dark conditions. Moreover, photoelectrode prepared from electropolymerization of 15 min (15-PPy/TiO_2) exhibited higher photocurrent density and OCP shift than other electrodes. In addition, the OCP was resumed after long time (1000 s) when light was cut off owing to the electron pool effect of PPy proving its sustained protection ability.

Recently, it was found that core−shell morphology can further enhances the PEC performance of PPy/TiO_2 nanorods in addition to higher visible light absorption and electron−hole separation efficiency [90]. As a result of core−shell structure large area is provided for p−n heterojunction and transmission of electrons which inhibits recombination of electron−hole pairs. PPy/TiO_2 nanorods film can shift the potential of coupled 304SS to −640 mV under the illumination of visible light. Moreover, due to the electron pool effect of PPy, the protection is maintained under dark condition.

PANI is also a conducting polymer having high stability and charge transfer ability. The composite photoanode of PANI/TiO_2 has higher PEC property and can enhance PCP. A ternary composite of TiO_2/graphene oxide/polyaniline (TO_2/GO/PANI) has been prepared and used as filler in epoxy resin (EP) [91]. The composite TiO_2/GO/PANI/EP provided better corrosion protection to Q235 CS. The photoanode exhibited very high photocurrent density (60 mA/cm^2) and shift in potential (−651 to −851 mV). The effective protection performance of TiO_2/GO/PANI/EP is due to the synergistic effect of PCP and physical passivation. As PANI has energy storage ability, the self-discharge of TO_2/GO/PANI releases electron providing protection even in the dark. Sodium polyacrylate/TiO_2 hybrid films also indicated enhanced photocurrent density and PCP performance. Under white light illumination, the hybrid films provided negative photopotential (−710 mV) for protection 304SS [92]. More recently, polythiophene (Pth) as a p-type semiconductor has been decorated on TNAs which increases light absorption and photocurrent density [93]. Pth/TNAs exhibited PCP for the attached 304SS in 3.5% NaCl solution and negatively shifting its potential (−670 mV). After decoration with Pth an increase in inner electric field occurs which promotes transfer of electrons to the coupled metal. This improves the charge separation and hence PEC performance resulting effective protection. In addition, in the dark, migration of electrons from metal to the composite semiconductor is prevented due to the galvanic effect barrier in 304SS/Ti interface and Schottky barrier in the Ti/semiconductor interface.

Table 26.1 shows the summary of TiO_2-based photoelectrodes for PCP of different types of metals. The OCP and photocurrent values given in the table are the maximum values among other values of different electrodes prepared. It is clear from the table that the maximum OCP value is 1100 for ZnS/CdSe/CdS/TiO_2 composite electrode. Very high photocurrent density was obtained for TiO_2/GO/PANI, ZnS−CdS−Ag@TiO_2, and PbS/TiO_2 photoelectrodes.

Although TiO_2 based photoelectrodes have received tremendous attention due to its high PEC performance and have been widely studied for PCP of metals, some other materials with effective

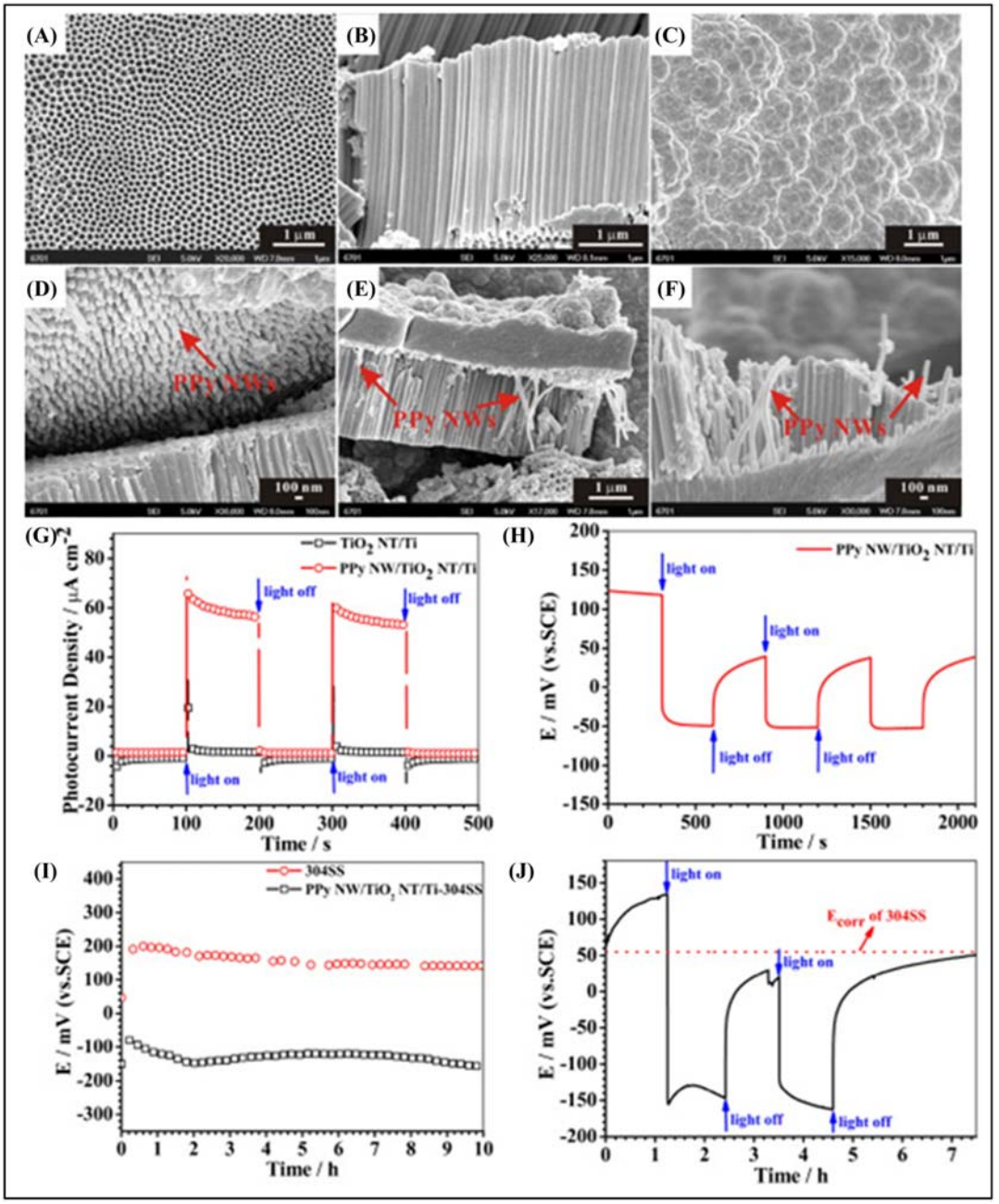

FIGURE 26.14

Field emission scanning electron microscopy (FESEM) images of top view (A) and cross-sectional view (B) of TiO_2 NTs as well as top view (C) and cross-sectional views (D–F) of the PPy NW/TiO_2 NT nanocomposite. (G) Photocurrent density versus time plots for TiO_2 NT/Ti and the PPy NW/TiO_2 NT nanocomposite-coated Ti electrode, (H) photoinduced OCP variation of PPy NW/TiO_2 NT nanocomposite-coated Ti, (I) OCP of pure 304SS electrode and 304SS connected to the PPy NW/TiO_2 NT/Ti nanocomposite photoanode, and (J) photoinduced OCP variation of 304SS electrode connected with PPy NW/TiO_2 NT/Ti nanocomposite in 3.5 wt. % NaCl solution under intermittent illumination with visible light ($\lambda > 420$ nm) [88].

Table 26.1 Summary of PCP performance of TiO_2-based photoelectrodes.

Photoanode	Light source[a]	Metal	Current density ($\mu A/cm^2$)	OCP (mV)	References
Pure TiO_2	SSL	304SS	260	–	[12]
H−TiO_2	SSL	304SS	1200	640	[12]
Pure TiO_2	SSL	304SS	400	630	[13]
UV−TiO_2	SSL	304SS	600	678	[13]
Fe−TiO_2	WL	304SS	–	360	[14]
Ag/Fe−TiO_2	Vis	403SS	230	700	[16]
W−Fe−TiO_2	Vis	403SS	680	530	[17]
Fe−Co−TiO_2	Vis	403SS	1112	470	[18]
Ni−Pt/Fe−TiO_2	SSL	403SS	250	541	[19]
Ni−TiO_2	Vis	304SS	14	370	[21]
Cr−TiO_2	SSL	316L SS	–	380	[24]
Ce−TiO_2	SSL	316L SS	–	180	[25]
N−TiO_2	UV	316L SS	–	470	[26]
B−TiO_2	Vis	403SS	1200	650	[29]
S−TiO_2	Vis	304SS	1100	370	[30]
N−F−TiO_2	Vis	304SS	–	515	[31]
ZnO−TiO_2	SSL	316SS/Q235 CS	151	991/1066	[33]
Fe_2O_3−TiO_2	SSL	CS	310	295	[37]
Pure TiO_2	Vis	304SS	70	330	
NiO−TiO_2	Vis	304SS	550	760	[38]
Cu_2O−TiO_2	Vis	316L SS	–	60	[39]
In_2O_3/TiO_2	Vis	304SS	180	600	[40]
β-Bi_2O_3/TiO_2	WL	403SS	80	450	[41]
CdS/TiO_2	WL	304SS	388	525	[43]
$CdTe/TiO_2$	Vis	304SS	400	850	[44]
$ZnSe/TiO_2$	Vis	304SS	–	780	[45]
$NiSe_2/TiO_2$	Vis	304SS	283	384	[46]
Ni_3S_2/TiO_2	Vis	304SS	53	720	[47]
Bi_2S_3/TiO_2	Vis	304SS	249	662	[49]
Bi_2Se_3/TiO_2	Vis	304SS	415	996	[50]
Ag_2S−TiO_2	Vis	304SS	30	840	[51]
PbS/TiO_2	Vis	304SS	3200	720	[53]
MnS/TiO_2	SSL	304SS	60	720	[54]
SnS/TiO_2	Vis	304SS	51	720	[55]
GQD/TiO_2	WL	304SS	800	740	[56]
CQD/TiO_2	SSL	Q235 CS	2280	620	[57]
CdSe/RGO/TiO_2	Vis	304SS	900	910	[58]
CdSe/graphene/TiO_2	Vis	304SS	560	750	[59]
PbS/CdS/$GTiO_2$	Vis	304SS	300	839	[60]

(*Continued*)

Table 26.1 Summary of PCP performance of TiO_2-based photoelectrodes. ***Continued***

Photoanode	Light source[a]	Metal	Current density ($\mu A/cm^2$)	OCP (mV)	References
TiO_2/CdS/PANI/G	SSL	304SS	340	844	[61]
TiO_2/$AgInS_2$/In_2S_3	SSL	316L SS	18	230	[62]
ZnS/Au/TiO_2	WL	403SS	–	400	[63]
ZnS−CdS−Ag@TiO_2	WL	403SS	19970	1174	[64]
CdTe/ZnS/TiO_2	WL	403SS	–	350	[65]
ZnS/CdSe/CdS/TiO_2	WL	403SS	–	1100	[66]
ZnS−Bi_2S_3/TiO_2/WO_3	WL	403SS	110	540	[67]
WO_3/TiO_2	Vis	304SS	2500	260	[71]
RGO/WO_3/TiO_2	Vis	304SS	590	760	[72]
WO_3−TiO_2−$BiVO_4$	Vis	304SS	27	625	[73]
SnO_2−TiO_2	UV	304SS	259	730	[77]
RGO/SnO_2/TiO_2	WL	304SS	310	590	[78]
Ag/SnO_2/TiO_2	Vis	304SS	195	990	[79]
MoO_3/TiO_2	WL	403SS	43	540	[82]
TiO_2/V_2O_5	UV	304SS	–	360	[83]
CNT/TiO_2	UV	304SS	18	610	[84]
Graphene/TiO_2	UV	304SS	100	600	[85]
Ag/graphene/TiO_2	Vis	304SS	221	640	[87]
PPy/TiO_2	Vis	304SS	28	640	[90]
TiO_2/GO/PANI	SSL	Q235 CS	60,000	851	[91]
Sodium polyacrylate/TiO_2	WL	SUS304 SS	8	710	[92]
Pth/TiO_2	Vis	304SS	800	380	[93]

[a]*Sources of light are simulated sunlight (SSL), visible light (Vis), white light (WL), and ultraviolet light (UV).*

PCP are needed to be explored. In this respect some photoelectrode materials other than TiO_2 have been recently investigated which are discussed below.

26.3 Zinc oxide photoelectrode

ZnO is n-type semiconductor material with a bang gap of 3.3 eV. Due to low cost, low toxicity, abundance, and high quantum efficiency make it suitable material and have applications in photocatalysis, solar cell, and electronic devices. ZnO is a promising material which can be applied for PEC cathodic protection of metals due to its high redox potential and electron mobility. It can be fabricated in the form of nanowires, nanorods, and nanoribbons for effective PEC performance. In addition, its energy band structure is also similar to that of TiO_2 while its CB potential is more negative than the corrosion potential of 304SS and Q235 CS and therefore can also be applied for PCP.

Yang et al. prepared ZnO nanorods on indium tin oxide (ITO) glass by electrodeposition with different deposition potentials [94]. The photoanode of ZnO nanorods prepared has unique surface nanostructure which renders it with high PEC activity. The photoanode can effectively protect 304SS and X52 CS in 3.5 wt.% NaCl solution under light illumination. The corrosion potential of 304SS and X52 CS negatively shifted to 306.6 and 39.1 mV, respectively, when coupled with ZnO photoanode. Moreover, they also prepared Co_3O_4@ZnO core−shell nanocomposites for enhanced PCP performance [95]. The composite photoanode shows red shift in optical absorption, high photocurrent density, and enhanced PCP performance as compared to ZnO nanorods. It can polarize the potential of 304SS to −720 mV under visible light (Fig. 26.15A). The enhanced performance is attributed to Co_3O_4, a p-type semiconductor with narrow band gap and formation of p−n junction at the interface improving charge separation as shown in Fig. 26.15B.

Recently, Liu et al. also reported the preparation of ZnO photoanodes at different temperatures and potentials resulting different morphologies for cathodic protection of 304SS in chloride solution under UV illumination [96,97]. ZnO NPs prepared at low temperature (40°C) are cauliflower-like and showed the best performance as compared to that obtained at higher temperature with other morphologies, such as rice-like nanorods (50°C) and hexagonal shape nanorods (60°C, 70°C, and 80°C). ZnO prepared at 40°C exhibited 10 times higher photocurrent density and more OCP shift of 304SS than others. ZnO NPs prepared at −0.7 and −1.0 V are hexagonal rods and those prepared at −1.6 V are spherical and show optimal PCP and higher OCP shift of 304SS under UV light illumination.

The high band gap of ZnO limits it application in visible light and therefore requires to be modified. It is shown that by coupling with graphene the band gap can be reduced to 1.17 eV which is due to the high conductivity of graphene with zero band gap. PCP performance of ZnOG was evaluated for 304SS and CS in NaCl and Na_2S solutions. ZnOG displayed effective corrosion

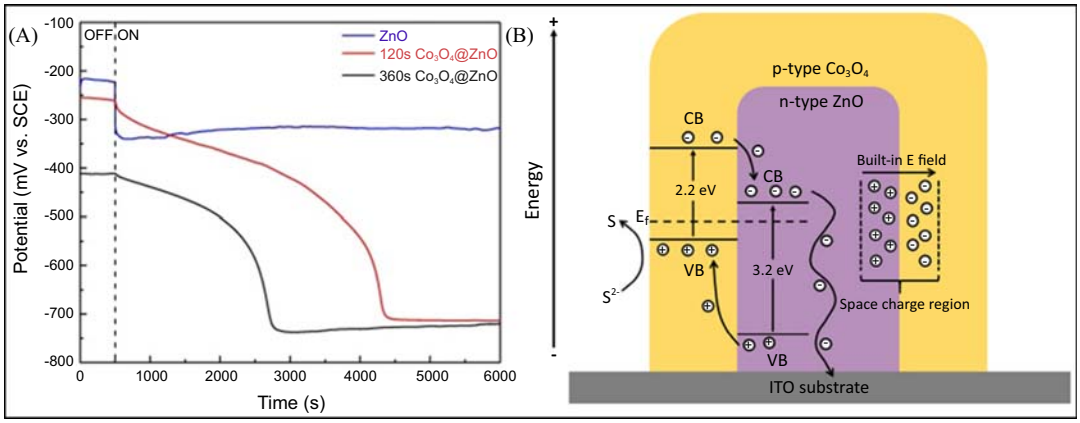

FIGURE 26.15

(A) Potential of the 304SS electrode in 3.5 wt.% NaCl solution when it is coupled with various prepared photoelectrodes under visible light illumination. (B) Schematic illustration of the p−n junction at the Co_3O_4/ZnO interface and the energy band structure of the prepared Co_3O_4@ZnO nanocomposite photoelectrodes [95].

protection for 304SS in the dark and UV light. CS can be effectively protected under UV illumination moving its potential to more negative (−870 mV vs SCE); however, it accelerates the corrosion of CS in NaCl solution under dark due to flow of electrons from its surface to ZnO.

Doping is an effective strategy to improve the PEC performance of ZnO due to the introduction of new energy level changing its band gap energy. Doping of metal increases the carrier concentration and results in improving PCP performance. Cobalt-doped ZnO indicated effective PCP of 316SS and Q235 CS in corrosive solution [98]. The PCP effect improved with increase in cobalt concentration and a ratio of 15% Co/Zn shows optimal results. The effective PCP performance of Co-doped ZnO is due to its intermediate energy level, narrow band gap, and improved separation of photogenerated electron−hole pairs.

The composite photoelectrode of In_2S_3/ZnO also indicated improved PCP for 304SS [99]. The composite photoanode caused potential drop of 304SS under visible light. Electrons from the VB of In_2S_3 are excited to CB under light illumination and then migrated to the 304SS shifting its potential to a negative region.

26.4 Graphitic carbon nitride photoelectrode

Graphitic carbon nitride (g-C_3N_4) is a metal-free semiconductor with a narrow band gap of 2.7 eV. It has many amazing properties such as low cost, ease of preparation, proper band structure, optical properties, low toxicity, and stability. It has been used in the field of photocatalysis such as photocatalytic degradation of pollutants, CO_2 reduction, and production of hydrogen and oxygen. Recently, g-C_3N_4 has also gained attention in the field PEC cathodic protection. For the first time, Bu et al. introduced g-C_3N_4 in the field of PEC cathodic protection of 304SS under visible and white light illumination [100]. The photogenerated electrons have enough energy to cross the barrier between thin film of g-C_3N_4 and 304SS generating current which leads to reduction of oxygen in the solution of NaCl. In addition to PCP property, g-C_3N_4 can also provide physical protection to the metal substrates due to its passivation.

Although g-C_3N_4 exhibits effective PCP performance, there are some issues which should be addressed. Because of its low CB potential (1.3 vs NHE, which is Normal Hydrogen Electrode), the photogenerated holes are not able to oxidize water easily. Moreover, there is also insufficient light absorption in visible region and fast recombination of electron−hole pairs. It is therefore necessary to modify g-C_3N_4 and to increase the depolarization efficiency of the photogenerated holes for effective PCP. In order to enhance its efficiency, Bu et al. prepared C_3N_4@ZnO core−shell composite photoanode [101]. The composite photoanode with 1% C_3N_4 indicated effective protection of 304SS shifting its OCP to −0.4 V under white light illumination. This is attributed to the formation of heterojunction electric field at the interface between C_3N_4 and ZnO which promotes the separation of electron−hole pairs. They also explored that PEC performance of the composite photoanode can be promoted by using oxygen doped C_3N_4 [102]. The prepared composite with core−shell structure O-C_3N_4@TiO_2 exhibited more photocurrent density, photocatalytic, and PEC performance than C_3N_4@TiO_2. It is due to the formation of chemical bonds between hydroxyl residues on the surface of TiO_2 and oxidizing groups on surface of O-C_3N_4. These bonds act as

transfer channels for electrons, which are captured from the VB of O-C_3N_4 improving charge separation and suppressing the recombination (Fig. 26.16).

The core−shell structure of C_3N_4@In_2O_3 also results in enhanced visible light absorption and PCP capability of 304SS under visible light [103]. Optimal PCP is obtained for C_3N_4@In_2O_3 composite with 3% C_3N_4. The formation of heterojunction at the interface between C_3N_4 and In_2O_3 improves the separation efficiency of photogenerated electron−hole pairs. The separation of photogenerated charge carriers was also improved by multilayer homojunction structure C_3N_4 which is prepared by rapid recrystallization technique [104]. The PEC cathodic protection of photoanode was evaluated for

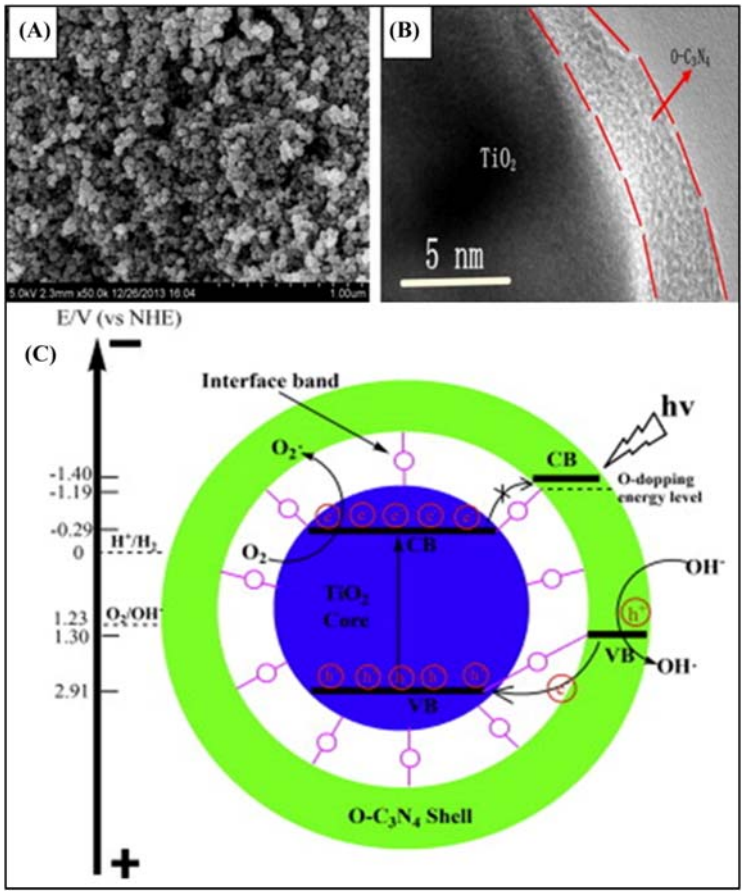

FIGURE 26.16

SEM (A) and HRTEM (B) morphologies of 3 wt.% O-C_3N_4@TiO_2 composite with quasishell core nanostructure. (C) Proposed mechanism for the promotion of the separation efficiency of the photoinduced electrons and holes generated by the O-C_3N_4@TiO_2 composite [102].

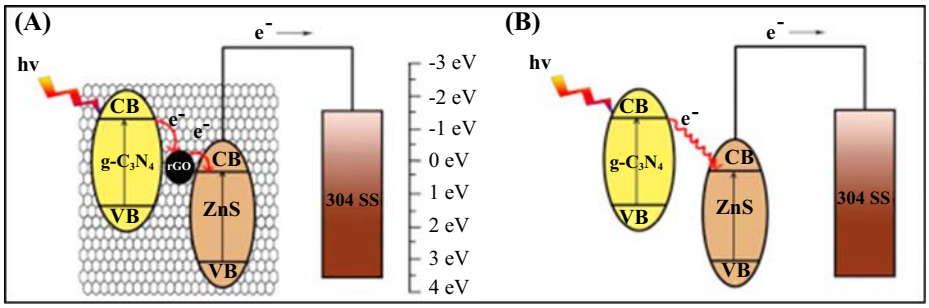

FIGURE 26.17

The photocathodic protection mechanism of 15%-rGO/g-C_3N_4/ZnS (A) and 0%-rGO/g-C_3N_4/ZnS (B) photoelectrode coupled with 304SS system [107].

CS droping its potential as low as −0.78 V which is due to the enhanced efficiency of photoinduced charge separation as a result of homojunction structure. The prepared photoanode also shows high stability and provides protection to coupled steel for 5 h. The effective protection under dark was also achieved by visible light active hybrid film of g-C_3N_4/TiO_2 [105]. The potential of 304SS electrode coupled with g-C_3N_4/TiO_2, dropped 200 mV under sunlight. The photopotential achieved during illumination can hold for many hours in the dark proving effective corrosion protection.

Recently, it was also noted that the change in morphology can also change the PEC activity of g-C_3N_4 [106].

Codoping of K and I can result not only change in the band structure of g-C_3N_4 but also to its n-type semiconductor. As a result, its band gap is narrowed which leads to more light absorption. 316L SS can be effectively protected in NaCl solution when couples with n-type g-C_3N_4. In another report, it was explored that a ternary composite electrode of g-C_3N_4/rGO/ZnS exhibits enhanced PCP performance and effectively protects 304SS from corrosion as compared to g-C_3N_4 [107]. When coupled to this composite electrode, the photoinduced photocurrent density of the steel reaches very high (2180 $\mu A/cm^2$) and is four times that of g-C_3N_4. The OCP of 304SS shifted negatively to 600 mV. In the composite photoelectrode, rGO acts as a mediator accelerating the electron transfer to ZnS from g-C_3N_4 and promotes the separation as indicated in Fig. 26.17.

26.5 Bismuth vanadate photoelectrode

Bismuth vanadate ($BiVO_4$) is also a promising semiconductor photoelectrode due to its narrow band gap (2.4 eV), high visible light harvesting, low cost, and stability. It has wide applications in the field of photocatalysis, pollutant degradation, photovoltaic devices, and water splitting. However, poor efficiency of light absorption, charge separation, and transmission affects it PEC performance. Thus it is necessary to improve its efficiency of photocatalytic activity. Different strategies have been adopted to improve performance of this photoelectrode such as morphology control, doping, and constructing heterojunction. Li et al. prepared porous $BiVO_4$ films which can provide effective cathodic protection to 316 steel under illumination decreasing its self-corrosion potential by 166 mV [108]. However, the

efficiency is limited by its relative position of the Fermi level. The PEC performance improved after decorating with $NiFeO_x$, an oxygen evolution reaction catalyst. The photoelectrode further shifted negatively the self-corrosion potential of 316 steel for about 90 mV. This is attributed to the reduced recombination of electron−hole pairs and transfer of more electrons from $BiVO_4$ to the steel. To improve light harvesting and photoinduced separation of charge carriers, CdSe QDs were used to fabricate $BiVO_4$/CdSe composite photoanode with heterojunction. The composite consists of pyramid shape $BiVO_4$ with CdSe QDs on its surface (Fig. 26.18) [109].

QDs as narrow band gap semiconductors and sensitizer can improve the PEC performance of photoelectrodes. The results indicated that composite photoanode provided boosted cathodic protection to 304SS increasing photocurrent density to 608 $\mu A/cm^2$ and potential drop of 708 mV, which are, respectively, 5.06 times and 2.10 times more than $BiVO_4$. This is attributed to the high oxygen

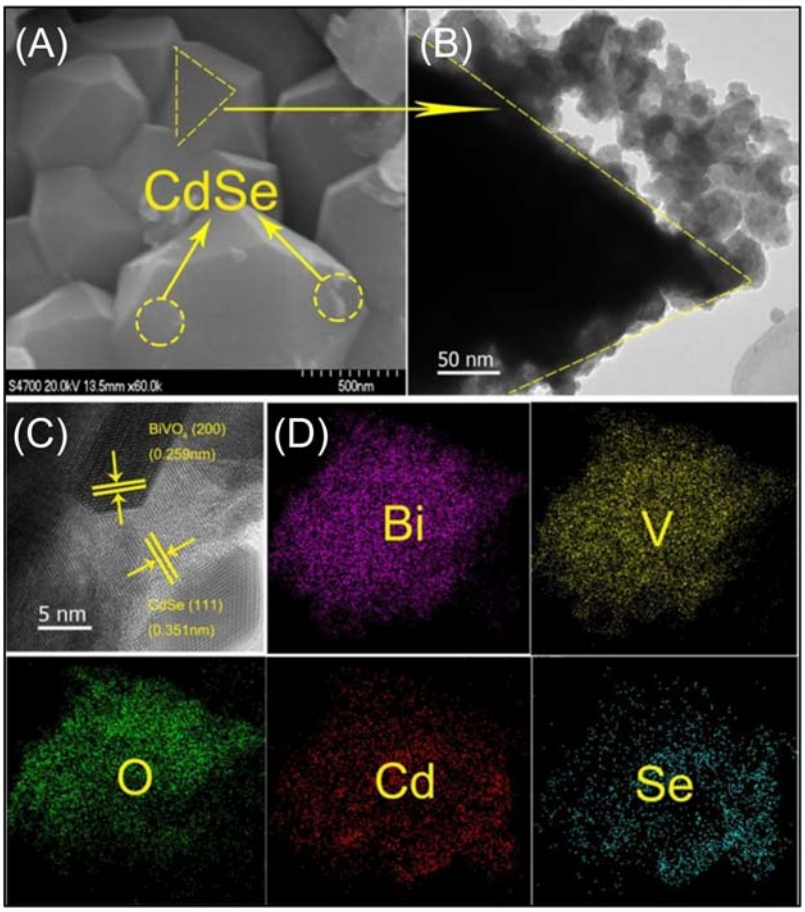

FIGURE 26.18

FESEM (A), TEM (B), and HRTEM (C) images and corresponds EDS elemental mapping (D) of 8V-BC [109].

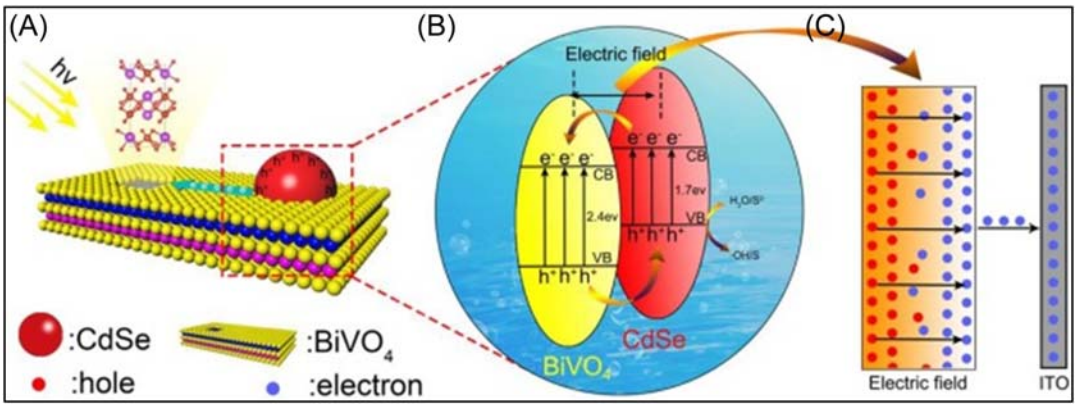

FIGURE 26.19

Architecture model of V-BC photoanode (A), energy band structure (B), and charge transfer mechanism (C) [109].

vacancies, visible light absorption, and carrier separation. In addition, the heterojunction at the interface between CdSe and $BiVO_4$ also promotes the efficiency of charge separation and transmission. Due to the narrow band gap (1.7 eV) of CdSe QDs, electrons easily excited and to it CB and then transferred to CB of $BiVO_4$ and subsequently to the coupled steel (Fig. 26.19).

Recently, Guo et al. prepared a ternary heterojunction composite photoanode of $WO_3/BiVO_4/Bi_2S_3$ which provided efficient PCP to 304SS [110]. The PEC results showed the OCP of 304SS in 3.5% NaCl solution dropped to − 690 mV when coupled with the composite photoanode. Moreover, the protection of metal could be maintained for long time of 10 h which is attributed to separation of charges and energy storage ability.

In addition to $BiVO_4$, there are also some other bismuth-based semiconductor materials such as bismuth sulfide (Bi_2S_3), bismuth selenide (Bi_2Se_3), oxyhalides (BiOX), and oxides (Bi_2WO_6, Bi_2MoO_6, $BiFeO_3$, Bi_2O_3, and $CuBi_2O_4$) which find applications in the field of PEC photocatalysis.

26.6 Strontium titanate photoelectrode

Strontium titanate ($SrTiO_3$) is n-type semiconductor with almost same band gap (3.2 eV) as that of TiO_2. As compared to TiO_2, its CB edge is 200 mV more negative and has high UV activity. It was noted that $SrTiO_3$ has photocatalytic water splitting activity under UV. Thus it is considered a promising material for PCP and can polarize metal to negative potential of stable region.

Ohko et al. investigated the PCP performance of $SrTiO_3$ films that were fabricated on ITO-coated glass using spray pyrolysis method [111]. It was found that CS can be effectively protected by the photoelectrode. The photopotential of electrode decreased more (−770 mV vs Ag/AgCl) than that of steel (−500 mV) in NaCl solution (3%), providing protection and prevention from

dissolution. Under UV light, photogenerated electrons are excited to the CB of $SrTiO_3$ and subsequently transmitted to the surface of CS causing its polarization. Yang et al. investigated different factors affecting the PCP performance of $SrTiO_3$ using two types of steels, X52 CS and 304SS [112]. It was found X52 CS can be protected under higher photocurrent density than 304SS, which is because of more positive CB potential of $SrTiO_3$ for 304SS than for CS. The photocurrent density is dependent upon the threshold area ratio of electrode and steel which is different for both steels with 8:1 and 1:1 for X52 CS and for 304SS, respectively. Na_2S is more effective hole scavenger than H_2O for both steels. Moreover, the photocurrent density increases with increasing light intensity and more protection is obtained. Since the band gap of $SrTiO_3$ is wide, its photocatalytic applications are restricted due to its response in UV region. In addition, the fast recombination of photoinduced charge carriers will affect PEC activity. In order to enhance its efficiency, some strategies have been adopted. Doping can introduce energy levels into the band gap which can expand the optical absorption to visible region. The donor or acceptor level caused by doping can reduce the band gap and semiconductor becomes sensitive to visible region. Cr-doped $SrTiO_3$ was prepared and treated with hydrogen to reduce the Cr^{6+} state to Cr^{3+} as the former has electron trapping ability [113]. Beside this Cr^{6+} can introduce level below the CB of semiconductor causing its CB to shift in positive direction which leads to decreased reduction ability of the photogenerated electrons. It was verified that hydrogen-treated Cr-doped $SrTiO_3$ indicated the presence of Cr^{3+}, an increase in charge carriers and effective charge transfer. Moreover, as a result of hydrogen treatment, oxygen vacancies are produced which led to negative shift in CB potential and more charge carrier concentration. The prepared photoanode exhibited effective PCP of 304SS under visible light illumination and excellent stability.

As stated earlier, the fast recombination of photogenerated electron−hole pairs leads to ineffective and short-term PCP, it is very urgent to make photoelectrodes to provide round the clock PCP. We know that CeO_2 has energy storage ability due to its multivalence nature. A bilayered CeO_2/$SrTiO_3$ composite photoanode was explored for efficient PCP [114]. The PEC properties of the composite electrode were studied and results showed that it can polarize the potential of 304SS in NaCl solution (3.5%) under light illumination. The self-discharge of CeO_2 can provide protection under dark for 7 h due to its electron storage property. The principle of metal protection both under illumination and dark conditions by the composite photoelectrode is schematically shown in Fig. 26.20. Under illumination, the photogenerated electrons are transferred to the metal while the holes are captured by S ions as indicated in Eq. (26.4)

$$SrTiO_3 \xrightarrow{UV} SrTiO_3 * \left(e^- + h^+\right) \tag{26.4}$$

$$S^{2-} + 2h^+ \rightarrow S \tag{26.5}$$

The electrons can be easily transferred from $SrTiO_3$ to the steel and cathodically polarize it due to the more negative CB potential of $SrTiO_3$ than that of corrosion potential of the 304SS. A part of photogenerated electrons are used in the reduction of CeO_2 and are stored in it during the charging process. In the dark conditions, the potential of steel still remains negative than its corrosion potential due to the discharging of composite photoelectrode and provides protection for long time (Fig. 26.20).

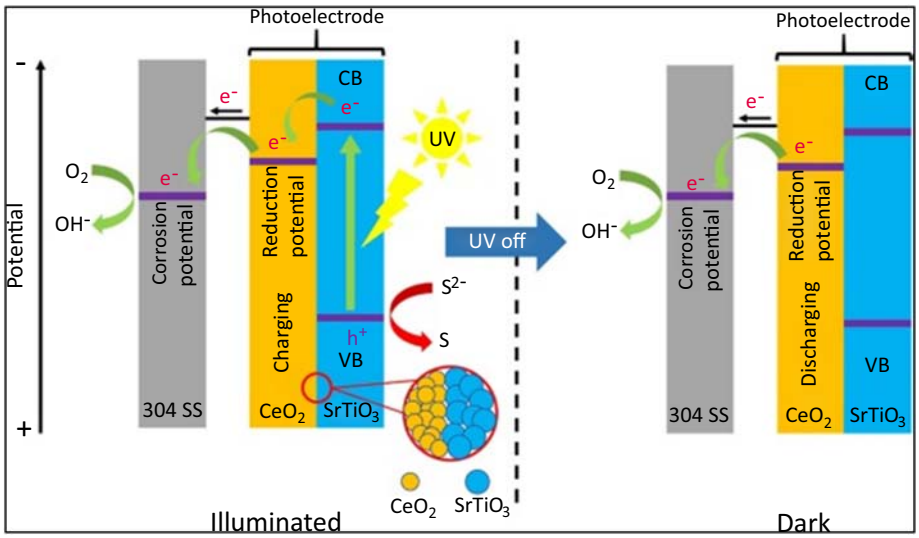

FIGURE 26.20

Schematic diagram of the principle of the bilayered $CeO_2/SrTiO_3$ nanocomposite photoelectrode for photoelectron storage and photocathodic protection of 304SS under illumination and in the darkness [114].

26.7 Hematite photoelectrode

Hematite (α-Fe_2O_3) is an n-type semiconductor with a narrow band gap (2.1 eV). Its high stability, abundance, nontoxicity visible light absorption, and ease of preparation make it suitable candidate for PEC applications. It has been applied for pollutants degradation and water splitting. In addition, its CB potential (−0.62 V vs SCE) is more negative than the self-corrosion potential of steel making this material suitable for PCP of steel. However, its application in photocatalysis is limited by its high charge carrier recombination, short diffusion length, and poor conductivity. Many strategies have been tried to enhance its PEC activity such as doping with metal and nonmetal, surface modification, heterojunction construction, coupling with catalyst, and morphology modification.

Nanostructuring and morphology modification can enhance the surface of the catalyst and hence its performance. Deng et al. fabricated nanotube arrays (NTA) of α-Fe_2O_3 on CS for its PCP [115]. The prepared α-Fe_2O_3 NTA exhibited high light absorption (up to 700 nm) and photoeffect. The potential of iron oxide prepared is more negative in NaCl solution both under light illumination and also more negative than CS. The CS covered with iron oxide NTA is protected and corrosion rate is slow as compared to bare steel. Xiong et al. explained the mechanism of PCP performance of α-Fe_2O_3 photoanode [116]. In the presence of Na_2S, scavenger with alkaline solution CS can be completely protected by α-Fe_2O_3 under light illumination. However, in the absence Na_2S, the corrosion can be delayed but not prevented which is due to the fast recombination of electron−hole pairs inhibiting the transfer of electrons to CS. Thus effective cathodic protection is not only

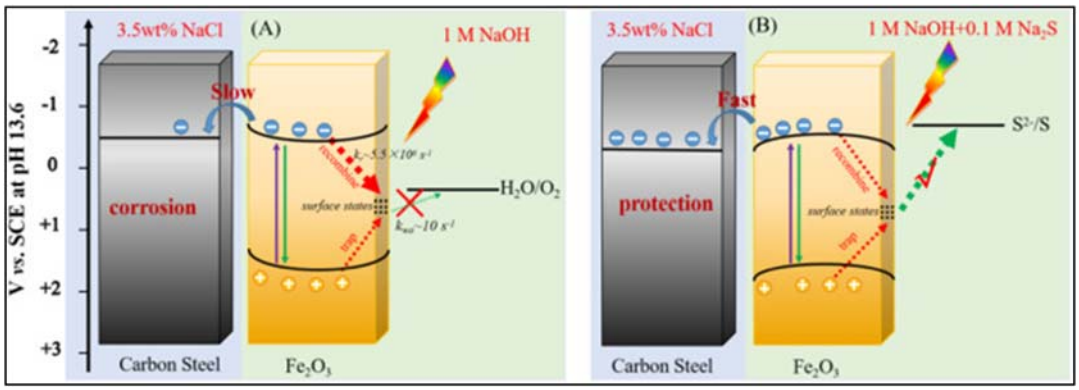

FIGURE 26.21

Scheme illustrations of the photoinduced corrosion (A) and protection (B) mechanism of α-Fe_2O_3 film following the photon absorption in 1 M NaOH and 1 M NaOH + 0.1 M Na_2S aqueous solution, respectively [116].

dependent upon the relative position of CB potential of photoanode and metal but also on the surface reaction dynamics (Fig. 26.21).

Visible light active photoanode of NiS/Fe_2O_3 was prepared through successive ionic layer adsorption and reaction (SILAR) technique using different cycles [117]. The prepared composite photoanode was used to inhibit the corrosion of 403SS. It was noted that the PEC activity of the composite is affected with number of SILAR cycles for NiS deposition. NiS/Fe_2O_3 shows more photocurrent density and more negative shift of corrosion potential than Fe_2O_3. The photoanode with five cycles showed the best PCP performance for 403SS in NaCl (3.5%) solution causing its potential to dropped by 200 mV as compared to its corrosion potential. This enhanced PCP is considered to be due to effective separation and transmission of charge.

An effective, stable and visible light responsive photoelectrode was obtained by combining α-Fe_2O_3 with $NiFe(OH)_x$ cocatalyst to obtain α-Fe_2O_3/$NiFe(OH)_x$ photoelectrode [118]. The PEC performance of composite electrode was greatly enhanced as compared to α-Fe_2O_3. Moreover, photopotential and self-corrosion potential of 304SS was shifted to more negative proving corrosion protection. OCP results indicated composite electrode shifted the potential of 304SS to −0.46 V under white illumination in the presence of chloride solution of NaCl. A stable photopotential was shown by composite electrode under illumination for 4 h and without any change in its morphology indicting improved photostability. The enhanced PCP performance of α-Fe_2O_3/$NiFe(OH)_x$ photoelectrode is actually due to reduced charge recombination and efficient electron transfer from photoelectrode to coupled 304SS.

Recently, Momeni et al. also deposited NiMoZn on hematite nanostructures (HNs) to produce NiMoZn/HN composite photoelectrode [119]. The composite electrode showed enhanced photocurrent density (510 μA/cm^2), five times higher than α-Fe_2O_3 and enhanced PCP performance. The OCP of 403SS decreased by −620 mV versus Ag/AgCl when coupled with composite photoelectrode which more than with Fe_2O_3 photoelectrode (−437 mV) proving its efficient corrosion protection.

26.8 Conclusion and future perspectives

Many technologies have been employed in order to prevent corrosion of the metals. However, PCP is one of the most efficient, green, and cost-effective techniques. Since semiconductor photoanode is an important part of PCP technique, many types of materials have been researched in this field such as TiO_2, ZnO, g-C_3N_4, $BiVO_4$, $SrTiO_3$, and α-Fe_2O_3. Among these, TiO_2 is the most widely studied semiconductor due to its promising properties. In order to enhance the efficiency, these materials have been modified using different materials. Although these materials indicate significant PCP performance, the efficiency of photoanodes still to be improved for practical applications. Moreover, there are still challenges in the field of PCP which should be resolved in future by considering the following points.

Some innovative architecture designs of multicocatalysts and TiO_2 are need to be fabricated for better PCP performance. The semiconductors having cocatalysts with both oxidizing and reducing agents can greatly enhance the separation of photogenerated charge carriers. Moreover, the spatially separated dual oxidation and reduction cocatalysts such as core−shell morphology of photocatalysts with one catalyst on one side and another on the other side can further enhance PEC performance due to the inhibition of recombination of chare carriers. The in-depth mechanism of photocatalytic active sites and migration pathways of charge carriers must also be investigated for structure fabrication of binary cocatalysts. The presence of hole scavengers, such as water that is oxidized by holes, is also important for charge separation. If the water oxidation rate is slow, holes will recombine with electrons making the process less effective. Thus reduction in the energy barrier of water oxidation has important role in PEC performance of the photoanode.

PCP potential is important for metal protection and more negative CB potential of the photoanode results in more negative polarization potential of the metal. It is, therefore, necessary to develop n-type semiconductors with more negative CB potential and with visible light response. Some materials with more negative potential values such as TiO_2 and $SrTiO_3$ have been studied but other materials with such property are also suggested to be researched.

Photocurrent density is also important factor which should be enhanced in order to improve PCP performance. There is direct relationship between the photocurrent density and PCP efficiency. More area can be protected with higher value of photocurrent density of the photoanode. By engineering, the band gap and energy barrier of the surface reaction photocurrent density can be modified.

Modification of photoanode with some conductive materials such as noble metals, conductive polymers, and carbon-based materials can improve charge transfer and PEC performance. However, conductive materials with negative work functions and their optimized amount will be needed for better results.

The most important problem with PCP is its inefficiency under dark. In order to minimize, this issue materials with electron storage ability and negative discharge potential such as WO_3 and SnO_2 have been developed. However, the efficiency of these materials is low and therefore some other materials with high electron storage capacity should be researched for modification of photoanodes. In addition, the mechanism of charge storage and charge transfer has not been fully researched which also needs to be explored for better PCP.

The combination of PCP and traditional methods for anticorrosion will lead to improved protection of metals as single technique may not be so effective. More research is required to develop

novel type of materials with dual functions. The combination of photoanodes and organic polymers with anticorrosion ability can result in effective protection. Organic polymers such as PPy, polyethyleneimine, and PANI have been studied. Some more organic polymers, ionic liquids, etc. need to be explored in this area. Composite materials of semiconductors and graphene can also be researched in this field. The design and surface modification of semiconductor for fabrication with polymers should be considered in future to get stable materials for PCP.

Various methods have been employed to construct semiconductors materials of various morphologies for PCP. However, most of the methods reported are complex and require precious materials for synthesis. More cheap materials and simple methods need to be explored for efficient PCP performance. The materials should be designed to be stable and active under harsh conditions.

References

[1] G. Koch, J. Varney, N. Thompson, O. Moghissi, M. Gould, J. Payer, International measures of prevention, application, and economics of corrosion technologies study, NACE Int. 216 (2016).

[2] F.E. Castillejo, D.M. Marulanda, J.J. Olaya, J.E. Alfonso, Wear and corrosion resistance of niobium–chromium carbide coatings on AISI D2 produced through TRD, Surf. Coat. Technol. 254 (2014) 104–111.

[3] A.E. Hughes, I.S. Cole, T.H. Muster, R.J. Varley, Designing green, self-healing coatings for metal protection, NPG Asia Mater. 2 (4) (2010) 143–151.

[4] W. Sun, Y. Liu, T. Li, S. Cui, S. Chen, Q. Yu, et al., Anti-corrosion of amphoteric metal enhanced by MAO/corrosion inhibitor composite in acid, alkaline and salt solutions, J. Colloid Interface Sci. 554 (2019) 488–499.

[5] S. Kainuma, M. Yang, S. Ishihara, A. Kaneko, T. Yamauchi, Corrosion protection of steel members using an Al-Zn base sacrificial anode and fiber sheet in an atmospheric environment, Constr. Build. Mater. 224 (2019) 880–893.

[6] H. Park, K.Y. Kim, W. Choi, Photoelectrochemical approach for metal corrosion prevention using a semiconductor photoanode, J. Phys. Chem. B 106 (18) (2002) 4775–4781.

[7] J. Yuan, S. Tsujikawa, Photo-effects of sol-gel derived TiO_2 coating on carbon steel in alkaline solution, Zairyo-to-Kankyo 44 (10) (1995) 534–542.

[8] J. Yuan, R. Fujisawa, S. Tsujikawa, Photopotentials of copper coated with TiO_2 by sol-gel method, Zairyo-to-Kankyo 43 (8) (1994) 433–440.

[9] H. Yun, C. Lin, J. Li, J. Wang, H. Chen, Low-temperature hydrothermal formation of a net-like structured TiO_2 film and its performance of photogenerated cathode protection, Appl. Surf. Sci. 255 (5) (2008) 2113–2117.

[10] N. Sakai, Y. Ebina, K. Takada, T. Sasaki, Electronic band structure of titania semiconductor nanosheets revealed by electrochemical and photoelectrochemical studies, J. Am. Chem. Soc. 126 (18) (2004) 5851–5858.

[11] C.-X. Lei, H. Zhou, C. Wang, Z.-D. Feng, Self-assembly of ordered mesoporous TiO_2 thin films as photoanodes for cathodic protection of stainless steel, Electrochim. Acta 87 (2013) 245–249.

[12] N. Wei, Y. Liu, T. Zhang, J. Liang, D. Wang, Hydrogenated TiO_2 nanotube arrays with enhanced photoelectrochemical property for photocathodic protection under visible light, Mater. Lett. 185 (2016) 81–84.

[13] T. Zhang, Y. Liu, J. Liang, D. Wang, Enhancement of photoelectrochemical and photocathodic protection properties of TiO_2 nanotube arrays by simple surface UV treatment, Appl. Surf. Sci. 394 (2017) 440–445.

[14] Y. Liu, C. Xu, Z.-D. Feng, Characteristics and anticorrosion performance of Fe-doped TiO_2 films by liquid phase deposition method, Appl. Surf. Sci. 314 (2014) 392−399.
[15] J. Li, H. Yun, C.-J. Lin, Investigations on the Fe-doped TiO_2 nanotube arrays as a photoanode for cathodic protection of stainless steel, ECS Trans. 3 (43) (2008) 1.
[16] M.M. Momeni, P. Zeinali, Fabrication of Ag electrodeposited-iron doped TiO_2 nanotube composites for photoelectrochemical cathodic protection applications, J. Electroanal. Chem. 891 (2021) 115283.
[17] M.M. Momeni, S.H. Khansari-Zadeh, H. Farrokhpour, Fabrication of tungsten-iron-doped TiO_2 nanotubes via anodization: new photoelectrodes for photoelectrochemical cathodic protection under visible light, SN Appl. Sci. 1 (10) (2019) 1−10.
[18] M.M. Momeni, M. Mahvari, Y. Ghayeb, Photoelectrochemical properties of iron-cobalt $WTiO_2$ nanotube photoanodes for water splitting and photocathodic protection of stainless steel, J. Electroanal. Chem. 832 (2019) 7−23.
[19] M.M. Momeni, Y. Ghayeb, N. Moosavi, Preparation of Ni−Pt/Fe−TiO_2 nanotube films for photoelectrochemical cathodic protection of 403 stainless steel, Nanotechnology 29 (42) (2018) 425701.
[20] M.M. Momeni, M. Motalebian, Y. Ghayeb, M. Atapour, Photoelectrochemical cathodic protection of stainless steel using W-and Cr-doped/codoped TiO_2 nanotube thin film photoanodes, J. Electrochem. Soc. 168 (8) (2021) 081504.
[21] M. Sun, Z. Chen, J. Yu, Highly efficient visible light induced photoelectrochemical anticorrosion for 304 SS by Ni-doped TiO_2, Electrochim. Acta 109 (2013) 13−19.
[22] L.-Y. Qiao, F.-Y. Xie, M.-H. Xie, C.-H. Gong, W.-L. Wang, J.-C. Gao, Characterization and photoelectrochemical performance of Zn-doped TiO_2 films by sol−gel method, Trans. Nonferrous Met. Soc. China 26 (8) (2016) 2109−2116.
[23] T. Zhang, B. Yu, D. Wang, F. Zhou, Molybdenum-doped and anatase/rutile mixed-phase TiO2 nanotube photoelectrode for high photoelectrochemical performance, J. Power Sources 281 (2015) 411−416.
[24] S. Li, J. Fu, Improvement in corrosion protection properties of TiO_2 coatings by chromium doping, Corros. Sci. 68 (2013) 101−110.
[25] S. Li, Q. Wang, T. Chen, Z. Zhou, Y. Wang, J. Fu, Study on cerium-doped nano-TiO_2 coatings for corrosion protection of 316 L stainless steel, Nanoscale Res. Lett. 7 (1) (2012) 1−9.
[26] J. Li, C.-J. Lin, Y.-K. Lai, R.-G. Du, Photogenerated cathodic protection of flower-like, nanostructured, N-doped TiO_2 film on stainless steel, Surf. Coat. Technol. 205 (2) (2010) 557−564.
[27] J. Li, H. Yun, C.-J. Lin, A photoelectrochemical study of n-doped TiO_2 nanotube arrays as the photoanodes for cathodic protection of SS, J. Electrochem. Soc. 154 (11) (2007) C631.
[28] P. Qiu, X. Sun, Y. Lai, P. Gao, C. Chen, L. Ge, N-doped TiO_2@TiO_2 visible light active film with stable and efficient photocathodic protection performance, J. Electroanal. Chem. 844 (2019) 91−98.
[29] M.M. Momeni, M. Taghinejad, Y. Ghayeb, R. Bagheri, Z. Song, Preparation of various boron-doped TiO_2 nanostructures by in situ anodizing method and investigation of their photoelectrochemical and photocathodic protection properties, J. Iran. Chem. Soc. 16 (9) (2019) 1839−1851.
[30] S. Arman, H. Omidvar, S. Tabaian, M. Sajjadnejad, S. Fouladvand, S. Afshar, Evaluation of nanostructured S-doped TiO_2 thin films and their photoelectrochemical application as photoanode for corrosion protection of 304 stainless steel, Surf. Coat. Technol. 251 (2014) 162−169.
[31] C.-X. Lei, Z.-D. Feng, H. Zhou, Visible-light-driven photogenerated cathodic protection of stainless steel by liquid-phase-deposited TiO_2 films, Electrochim. Acta 68 (2012) 134−140.
[32] H. Xu, W. Liu, L. Cao, G. Su, R. Duan, Preparation of porous TiO_2/ZnO composite film and its photocathodic protection properties for 304 stainless steel, Appl. Surf. Sci. 301 (2014) 508−514.
[33] X. Zhang, G. Chen, W. Li, D. Wu, Preparation and photocathodic protection properties of ZnO/TiO_2 heterojunction film under simulated solar light, Materials 12 (23) (2019) 3856.
[34] S. Boukerche, A. Himour, M. Bououdina, F. Bensouici, S. Ouchenane, Multilayered ZnO/TiO_2 nanostructures as efficient corrosion protection for stainless steel 304, Mater. Res. Express 6 (5) (2019) 055052.

[35] H.M. Abd El-Lateef, A.O. Alnajjar, M.M. Khalaf, Advanced self-healing coatings based on ZnO, TiO_2, and ZnO-TiO_2/polyvinyl chloride nanocomposite systems for corrosion protection of carbon steel in acidic solutions containing chloride, J. Taiwan Inst. Chem. Eng. 116 (2020) 286–302.
[36] J. Xue, J. Gao, Q. Shen, Q. Li, X. Liu, H. Jia, et al., Performance of photocatalytic cathodic protection of 20 steel by α-Fe_2O_3/TiO_2 system, Surf. Coat. Technol. 385 (2020) 125445.
[37] J. Cui, Y. Pei, Compounds, enhanced photocathodic protection performance of Fe_2O_3/TiO_2 heterojunction for carbon steel under simulated solar light, J. Alloy Compd. 779 (2019) 183–192.
[38] C. Han, Q. Shao, J. Lei, Y. Zhu, S. Ge, Compounds, preparation of NiO/TiO_2 p-n heterojunction composites and its photocathodic protection properties for 304 stainless steel under simulated solar light, J. Alloy Compd. 703 (2017) 530–537.
[39] J. Tian, Z. Chen, J. Jing, C. Feng, M. Sun, W. Li, Photoelectrochemical cathodic protection of Cu_2O/TiO_2 p-n heterojunction under visible light, J. Oceanol. 38 (2020) 1517–1531.
[40] M. Sun, Z. Chen, Enhanced photoelectrochemical cathodic protection performance of the In_2O_3/TiO_2 composite, J. Electrochem. Soc. 162 (3) (2014) C96.
[41] Z.-C. Guan, H.-P. Wang, X. Wang, J. Hu, R.-G. Du, Fabrication of heterostructured β-Bi_2O_3-TiO_2 nanotube array composite film for photoelectrochemical cathodic protection applications, Corros. Sci. 136 (2018) 60–69.
[42] J. Li, C.-J. Lin, J.-T. Li, Z.-Q. Lin, A photoelectrochemical study of CdS modified TiO_2 nanotube arrays as photoanodes for cathodic protection of stainless steel, Thin Solid Films 519 (16) (2011) 5494–5502.
[43] A. Boonserm, C. Kruehong, V. Seithtanabutara, A. Artnaseaw, P. Kwakhong, Photoelectrochemical response and corrosion behavior of CdS/TiO_2 nanocomposite films in an aerated 0.5 M NaCl solution, Appl. Surf. Sci. 419 (2017) 933–941.
[44] X.-T. Wang, Q.-Y. Wei, L. Zhang, H.-F. Sun, H. Li, Q.-X. Zhang, CdTe/TiO_2 nanocomposite material for photogenerated cathodic protection of 304 stainless steel, Mater. Sci. 208 (2016) 22–28.
[45] L. Zhang, X.-T. Wang, F.-G. Liu, H.-F. Sun, H. Li, Q.-Y. Wei, et al., Photogenerated cathodic protection of 304SS by ZnSe/TiO_2 NTs under visible light, Mater. Lett. 143 (2015) 116–119.
[46] X.-T. Wang, Q.-Y. Wei, J.-R. Li, H. Li, Q.-X. Zhang, S.-S. Ge, Preparation of $NiSe_2$/TiO_2 nanocomposite for photocathodic protection of stainless steel, Mater. Lett. 185 (2016) 443–446.
[47] Y. Nan, X. Wang, X. Ning, J. Lei, S. Guo, Y. Huang, et al., Fabrication of Ni_3S_2/TiO_2 photoanode material for 304 stainless steel photocathodic protection under visible light, Surf. Coat. Technol. 377 (2019) 124935.
[48] J. Hu, Z.-C. Guan, Y. Liang, J.-Z. Zhou, Q. Liu, H.-P. Wang, et al., Bi_2S_3 modified single crystalline rutile TiO_2 nanorod array films for photoelectrochemical cathodic protection, Corros. Sci. 125 (2017) 59–67.
[49] H. Li, X. Wang, Q. Wei, B. Hou, Photocathodic protection of 304 stainless steel by Bi_2S_3/TiO_2 nanotube films under visible light, Nanoscale Res. Lett. 12 (1) (2017) 1–6.
[50] W. Wang, X. Wang, N. Wang, X. Ning, H. Li, D. Lu, et al., Bi_2Se_3 sensitized TiO_2 nanotube films for photogenerated cathodic protection of 304 stainless steel under visible light, Nanoscale Res. Lett. 13 (1) (2018) 1–9.
[51] X.-B. Ning, S.-S. Ge, X.-T. Wang, H. Li, X.-R. Li, X.-Q. Liu, et al., Compounds, Preparation and photocathodic protection property of Ag_2S-TiO_2 composites, J. Alloy. Compd. 719 (2017) 15–21.
[52] Y. Yang, W. Zhang, Y. Xu, H. Sun, X. Wang, Ag_2S decorated TiO_2 nanosheets grown on carbon fibers for photoelectrochemical protection of 304 stainless steel, Appl. Surf. Sci. 494 (2019) 841–849.
[53] H. Guo, L. Li, C. Su, D. Yu, Z. Liu, Effective photocathodic protection for 304 stainless steel by PbS quantum dots modified TiO_2 nanotubes, Mater. Chem. Phys. 258 (2021) 123914.
[54] S.-S. Ge, Q.-X. Zhang, X.-T. Wang, H. Li, L. Zhang, Q.-Y. Wei, Photocathodic protection of 304 stainless steel by MnS/TiO_2 nanotube films under simulated solar light, Surf. Coat. Technol. 283 (2015) 172–176.

[55] J. Shao, Z.-D. Zhang, X.-T. Wang, X.-D. Zhao, X.-B. Ning, J. Lei, et al., Synthesis and photocathodic protection properties of nanostructured SnS/TiO_2 composites, J. Electrochem. Soc. 165 (10) (2018) H601.
[56] B. Qian, H. Dai, S. Tang, Z. Song, Enhanced photocathodic protection performance of graphene quantum dots sensitized TiO_2 nanotube arrays for 304 stainless steel, Optik 178 (2019) 128–134.
[57] M. Feng, Y. Liu, S. Zhang, Y. Liu, N. Luo, D. Wang, Carbon quantum dots (CQDs) modified TiO_2 nanorods photoelectrode for enhanced photocathodic protection of Q235 carbon steel, Corros. Sci. 176 (2020) 108919.
[58] H. Li, X. Wang, L. Zhang, B. Hou, Preparation and photocathodic protection performance of CdSe/reduced graphene oxide/TiO_2 composite, Corros. Sci. 94 (2015) 342–349.
[59] H. Li, X. Wang, L. Zhang, B. Hou, CdTe and graphene co-sensitized TiO_2 nanotube array photoanodes for protection of 304SS under visible light, Nanotechnology 26 (15) (2015) 155704.
[60] Y. Yang, W. Zhang, Y. Xu, H. Sun, Preparation of PbS and CdS cosensitized graphene/TiO_2 nanosheets for photoelectrochemical protection of 304 stainless steels, Appl. Surf. Sci. 452 (2018) 58–66.
[61] D. Xu, M. Yang, Y. Liu, R. Zhu, X. Lv, C. Zhang, et al., Fabrication of an innovative designed TiO_2 nanosheets/CdSe/polyaniline/graphene quaternary composite and its application as in-situ photocathodic protection coatings on 304SS, J. Alloy Compd. 822 (2020) 153685.
[62] M. Sun, Z. Chen, J. Li, J. Hou, F. Xu, L. Xu, et al., Enhanced visible light-driven activity of TiO_2 nanotube array photoanode co-sensitized by "green" $AgInS_2$ photosensitizer and In_2S_3 buffer layer, Electrochim. Acta 269 (2018) 429–440.
[63] Y.-F. Zhu, J. Zhang, L. Xu, Y. Guo, X.-P. Wang, R.-G. Du, et al., Fabrication and photoelectrochemical properties of ZnS/Au/TiO_2 nanotube array films, Phys. Chem. Chem. Phys. 15 (11) (2013) 4041–4048.
[64] Y. Zhu, Y. Liu, Z. Yang, Highly efficient photo-induced cathodic protection of 403SS by the all-solid-state Z-scheme ZnS-CdS-Ag@TiO_2 nanoheterojunctions, Int. J. Electrochem. Sci. 14 (2019) 815–825.
[65] J. Zhang, J. Hu, Y.-F. Zhu, Q. Liu, H. Zhang, R.-G. Du, et al., Fabrication of CdTe/ZnS core/shell quantum dots sensitized TiO_2 nanotube films for photocathodic protection of stainless steel, Corros. Sci. 99 (2015) 118–124.
[66] J. Zhang, R.-G. Du, Z.-Q. Lin, Y.-F. Zhu, Y. Guo, H.-Q. Qi, et al., Highly efficient CdSe/CdS co-sensitized TiO_2 nanotube films for photocathodic protection of stainless steel, Electrochim. Acta 83 (2012) 59–64.
[67] Z.-C. Guan, X. Wang, P. Jin, Y.-Y. Tang, H.-P. Wang, G.-L. Song, et al., Enhanced photoelectrochemical performances of ZnS-Bi_2S_3/TiO_2/WO_3 composite film for photocathodic protection, Corros. Sci. 143 (2018) 31–38.
[68] M.-J. Zhou, Z.-O. Zeng, L. Zhong, Photogenerated cathode protection properties of nano-sized TiO_2/WO_3 coating, Corros. Sci. 51 (6) (2009) 1386–1391.
[69] Y. Liang, Z.-C. Guan, H.-P. Wang, R.-G. Du, Enhanced photoelectrochemical anticorrosion performance of WO_3/TiO_2 nanotube composite films formed by anodization and electrodeposition, Electrochem. Commun. 77 (2017) 120–123.
[70] S. Yu, Y. Ling, R. Wang, J. Zhang, F. Qin, Z. Zhang, Constructing superhydrophobic WO_3@TiO_2 nanoflake surface beyond amorphous alloy against electrochemical corrosion on iron steel, Appl. Surf. Sci. 436 (2018) 527–535.
[71] W. Sun, S. Cui, N. Wei, S. Chen, Y. Liu, D. Wang, Hierarchical WO_3/TiO_2 nanotube nanocomposites for efficient photocathodic protection of 304 stainless steel under visible light, J. Alloy Compd. 749 (2018) 741–749.
[72] W. Liu, T. Du, Q. Ru, S. Zuo, Y. Cai, C. Yao, Preparation of graphene/WO_3/TiO_2 composite and its photocathodic protection performance for 304 stainless steel, Mater. Res. Bull. 102 (2018) 399–405.
[73] Y. Yang, Y. Cheng, Visible light illuminated high-performance WO_3-TiO_2-$BiVO_4$ nanocomposite photoanodes capable of energy self-storage for photo-induced cathodic protection, Corros. Sci. 164 (2020) 108333.

[74] R. Subasri, T. Shinohara, Investigations on SnO_2-TiO_2 composite photoelectrodes for corrosion protection, Electrochem. Commun. 5 (10) (2003) 897–902.
[75] R. Subasri, T. Shinohara, K. Mori, Modified TiO_2 coatings for cathodic protection applications, Sci. Technol. Adv. Mater. 6 (5) (2005) 501.
[76] M.J. Zhou, Z.O. Zeng, L.J. Zhong, corrosion, Energy storage ability and anti-corrosion protection properties of TiO_2-SnO_2 system, Mater. Corros. 61 (4) (2010) 324–327.
[77] J. Zhang, Z.U. Rahman, Y. Zheng, C. Zhu, M. Tian, D. Wang, Nanoflower like SnO_2-TiO_2 nanotubes composite photoelectrode for efficient photocathodic protection of 304 stainless steel, Appl. Surf. Sci. 457 (2018) 516–521.
[78] W. Liu, K. Yin, F. He, Q. Ru, S. Zuo, C. Yao, A highly efficient reduced graphene oxide/SnO_2/TiO_2 composite as photoanode for photocathodic protection of 304 stainless steel, Mater. Res. Bull. 113 (2019) 6–13.
[79] H. Li, X. Wang, Y. Liu, B. Hou, Ag and SnO_2 co-sensitized TiO_2 photoanodes for protection of 304SS under visible light, Corros. Sci. 82 (2014) 145–153.
[80] H.-P. Wang, Z.-C. Guan, H.-Y. Shi, X. Wang, P. Jin, G.-L. Song, et al., Ag/SnO_2/TiO_2 nanotube composite film used in photocathodic protection for stainless steel, J. Photochem. 417 (2021) 113353.
[81] R. Subasri, S. Deshpande, S. Seal, T. Shinohara, Evaluation of the performance of TiO_2-CeO_2 bilayer coatings as photoanodes for corrosion protection of copper, Electrochem. Solid State Lett. 9 (1) (2005) B1.
[82] Q. Liu, J. Hu, Y. Liang, Z.-C. Guan, H. Zhang, H.-P. Wang, et al., Preparation of MoO_3/TiO_2 composite films and their application in photoelectrochemical anticorrosion, J. Electrochem. Soc. 163 (9) (2016) C539.
[83] M.J. Zhou, N. Zhang, L. Zhang, J. Yan, Photocathodic protection properties of $TiO_2-V_2O_5$ composite coatings, Mater. Corros. 64 (11) (2013) 996–1000.
[84] W. Liu, Y. Wang, G. Su, L. Cao, M. Sun, X. Guo, et al., The effect of incorporating carbon nanotubes in titania films used for the photocathode protection of 304 stainless steel, Carbon 50 (10) (2012) 3641–3648.
[85] X. Guo, W. Liu, L. Cao, G. Su, H. Xu, B. Liu, Graphene incorporated nanocrystalline TiO_2 films for the photocathodic protection of 304 stainless steel, Appl. Surf. Sci. 283 (2013) 498–504.
[86] W. Zhang, H. Guo, H. Sun, R.-C. Zeng, Hydrothermal synthesis and photoelectrochemical performance enhancement of TiO_2/graphene composite in photo-generated cathodic protection, Appl. Surf. Sci. 382 (2016) 128–134.
[87] H. Li, X. Wang, Q. Wei, X. Liu, Z. Qian, B. Hou, Enhanced photocathodic protection performance of Ag/graphene/TiO_2 composite for 304SS under visible light, Nanotechnology 28 (22) (2017) 225701.
[88] S. Cui, X. Yin, Q. Yu, Y. Liu, D. Wang, F. Zhou, Polypyrrole nanowire/TiO_2 nanotube nanocomposites as photoanodes for photocathodic protection of Ti substrate and 304 stainless steel under visible light, Corros. Sci. 98 (2015) 471–477.
[89] J. Ren, B. Qian, J. Li, Z. Song, L. Hao, J. Shi, Highly efficient polypyrrole sensitized TiO_2 nanotube films for photocathodic protection of Q235 carbon steel, Corros. Sci. 111 (2016) 596–601.
[90] Y. Liu, C. Zhao, X. Wang, H. Xu, H. Wang, X. Zhao, et al., Preparation of PPy/TiO_2 core-shell nanorods film and its photocathodic protection for 304 stainless steel under visible light, Mater. Res. Bull. 124 (2020) 110751.
[91] S. Chen, B. Li, R. Xiao, H. Luo, S. Yu, J. He, et al., Design an epoxy coating with TiO_2/GO/PANI nanocomposites for enhancing corrosion resistance of Q235 carbon steel, Materials 14 (10) (2021) 2629.
[92] C. Lei, Y. Liu, H. Zhou, Z. Feng, R. Du, Photogenerated cathodic protection of stainless steel by liquid-phase-deposited sodium polyacrylate/TiO_2 hybrid films, Corros. Sci. 68 (2013) 214–222.
[93] Y. Xu, W. Zhang, W. Yu, J. Ding, H. Sun, Polythiophene-sensitized TiO_2 nanotube arrays for photogenerated cathodic protection of 304 stainless steel, J. Mater. Sci. 56 (6) (2021) 4470–4483.

[94] Y. Yang, Y. Cheng, One-step facile preparation of ZnO nanorods as high-performance photoanodes for photoelectrochemical cathodic protection, Electrochim. Acta 276 (2018) 311–318.
[95] Y. Yang, W. Cheng, Y. Cheng, Preparation of Co_3O_4@ZnO core-shell nanocomposites with intrinsic p-n junction as high-performance photoelectrodes for photoelectrochemical cathodic protection under visible light, Appl. Surf. Sci. 476 (2019) 815–821.
[96] Y. Liu, Z. Zhu, Y. Cheng, B. Wei, Y. Cheng, Effect of eletrodeposition temperature on the thin films of ZnO nanoparticles used for photocathodic protection of SS304, J. Electroanal. Chem. 881 (2021) 114945.
[97] Y. Liu, Z. Zhu, Y. Cheng, An in-depth study of photocathodic protection of SS304 steel by electrodeposited layers of ZnO nanoparticles, Surf. Coat. Technol. 399 (2020) 126158.
[98] X. Zhang, G. Chen, W. Li, D. Wu, Photocathodic protection of cobalt doped ZnO nanorod arrays for 316 stainless steel and Q235 carbon steel in 3.5 wt.% NaCl solution, Coatings 9 (12) (2019) 803.
[99] J. Jing, Z. Chen, Y. Bu, Visible light induced photoelectrochemical cathodic protection for 304 SS by In_2S_3-sensitized ZnO nanorod array, Int. J. Electrochem. Sci. 10 (2015) 8783–8796.
[100] Y. Bu, Z. Chen, J. Yu, W. Li, A novel application of g-C_3N_4 thin film in photoelectrochemical anticorrosion, Electrochim. Acta 88 (2013) 294–300.
[101] Y. Bu, Z. Chen, Highly efficient photoelectrochemical anticorrosion performance of C_3N_4@ZnO composite with quasi-shell–core structure on 304 stainless steel, RSC Adv. 4 (85) (2014) 45397–45406.
[102] Y. Bu, Z. Chen, Effect of oxygen-doped C_3N_4 on the separation capability of the photoinduced electron-hole pairs generated by O-C_3N_4@TiO_2 with quasi-shell-core nanostructure, Electrochim. Acta 144 (2014) 42–49.
[103] M. Sun, Z. Chen, Y. Bu, compounds, Enhanced photoelectrochemical cathodic protection performance of the C_3N_4@In_2O_3 nanocomposite with quasi-shell–core structure under visible light, J. Alloy Compd. 618 (2015) 734–741.
[104] W. Li, Y. Wang, X. Yang, F. Liu, W. Li, Graphitic carbon nitride prepared by rapid recrystallization for photoelectrochemical anticorrosion, ACS Appl. Nano Mater. 2 (12) (2019) 7559–7565.
[105] D. Ding, Q. Hou, Y. Su, Q. Li, L. Liu, J. Jing, et al., g-C_3N_4/TiO_2 hybrid film on the metal surface, a cheap and efficient sunlight active photoelectrochemical anticorrosion coating, J. Mater. Sci. Mater. Electron. 30 (13) (2019) 12710–12717.
[106] J. Jing, Z. Chen, C. Feng, M. Sun, J. Hou, Compounds, transforming g-C_3N_4 from amphoteric to n-type semiconductor: the important role of p/n type on photoelectrochemical cathodic protection, J. Alloy Compd. 851 (2021) 156820.
[107] H. Zheng, Y. Liu, Y. Zhou, D. Zhao, D. Wang, L. Yun, et al., Improved photocathodic protection performance of g-C_3N_4/rGO/ZnS for 304 stainless steel, J. Phys. Chem. Solids 148 (2021) 109672.
[108] Y. Li, J. Wang, S. Li, Y. Wu, J. Wang, F. Cao, et al., Solar energy protects steels against corrosion: enhanced protection capability achieved by NiFeOx decorated $BiVO_4$ photoanode, Mater. Res. Bull. 107 (2018) 416–420.
[109] D. Xu, Y. Liu, Y. Zhang, Z. Shi, M. Yang, C. Zhang, et al., Fabrication of pyramid-$BiVO_4$/CdSe composite with controlled surface oxygen vacancies boosting efficient carriers' separation for photocathodic protection, Chem. Eng. J. 393 (2020) 124693.
[110] H. Guo, Y. Zhang, S. Wang, L. Li, W. Wang, Q. Sun, In-situ generation of Bi_2S_3 to construct WO_3/$BiVO_4$/Bi_2S_3 heterojunction for photocathodic protection of 304SS, J. Electroanal. Chem. (2022) 116033.
[111] Y. Ohko, S. Saitoh, T. Tatsuma, A. Fujishima, Photoelectrochemical anticorrosion effect of $SrTiO_3$ for carbon steel, Electrochem. Solid State Lett. 5 (2) (2001) B9.
[112] Y. Yang, Y. Cheng, Factors affecting the performance and applicability of $SrTiO_3$ photoelectrodes for photoinduced cathodic protection, J. Electrochem. Soc. 164 (14) (2017) C1067.

[113] J. Jing, Z. Chen, Y. Bu, M. Sun, W. Zheng, W. Li, Significantly enhanced photoelectrochemical cathodic protection performance of hydrogen treated Cr-doped $SrTiO_3$ by Cr^{6+} reduction and oxygen vacancy modification, Electrochim. Acta 304 (2019) 386–395.
[114] Y. Yang, Y. Cheng, Bi-layered $CeO_2/SrTiO_3$ nanocomposite photoelectrode for energy storage and photocathodic protection, Electrochim. Acta 253 (2017) 134–141.
[115] H. Deng, M.-C. Huang, W.-H. Weng, J.-C. Lin, Technology, photocathodic protection of iron oxide nanotube arrays fabricated on carbon steel, Surf. Coat. Technol. 266 (2015) 183–187.
[116] X. Xiong, L. Fan, X. Zhang, C. Zhang, Y. Chu, J. Li, et al., Online image monitoring and kinetics study on photocathodic protection of carbon steel using α-Fe_2O_3 photoanode, J. Electroanal. Chem. 880 (2021) 114857.
[117] M.M. Momeni, Y. Ghayeb, M. Akbarnia, Z. Barati, Successive ionic layer adsorption and reaction (SILAR) deposition of nickel sulfide on the Fe_2O_3 nanotube for efficient photocathodic protection of stainless steel under visible light, J. Iran. Chem. Soc. 17 (12) (2020) 3367–3374.
[118] L. Fan, X. Zhang, C. Zhang, J. Li, C. Wu, Y. Chu, et al., A highly efficient α-$Fe_2O_3/NiFe(OH)_x$ photoelectrode for photocathodic protection of 304 stainless steel under visible light, Surf. Coat. Technol. 403 (2020) 126407.
[119] M.M. Momeni, M. Akbarnia, Photo-assisted electrodeposition of NiMoZn on hematite nanostructures and their photoelectrochemical application as photoanode for corrosion protection of stainless steel, J. Alloy Compd. 856 (2021) 158254.